Author Manuscript

Author Manuscript

Author Manuscript

Author Manuscript

HHS Public Access

Author manuscript

Cell Rep. Author manuscript; available in PMC 2022 March 29.

Published in final edited form as:

Cell Rep. 2022 February 22; 38(8): 110416. doi:10.1016/j.celrep.2022.110416.

Astrocyte-neuron crosstalk through Hedgehog signaling mediates cortical synapse development

Yajun Xie[1,6], **Aaron T. Kuan**[1], **Wengang Wang**[2], **Zachary T. Herbert**[3], **Olivia Mosto**[1], **Olubusola Olukoya**[1], **Manal Adam**[1,6], **Steve Vu**[1], **Minsu Kim**[1], **Diana Tran**[1], **Nicolás Gómez**[1], **Claire Charpentier**[1], **Ingie Sorour**[1], **Tiara E. Lacey**[1], **Michael Y. Tolstorukov**[4], **Bernardo L. Sabatini**[2], **Wei-Chung Allen Lee**[1,5], **Corey C. Harwell**[1,6,7,*]

[1]Department of Neurobiology, Harvard Medical School, Boston, MA 02115, USA

[2]Howard Hughes Medical Institute, Department of Neurobiology, Harvard Medical School, Boston, MA 02115, USA

[3]Molecular Biology Core Facilities, Dana-Farber Cancer Institute, Boston, MA 02215, USA

[4]Department of Informatics and Analytics, Dana-Farber Cancer Institute, Boston, MA 02215, USA

[5]F.M. Kirby Neurobiology Center, Boston Children's Hospital, Boston, MA 02115, USA

[6]Present address: Eli and Edythe Broad Center of Regeneration Medicine and Stem Cell Research, Department of Neurology, University of California San Francisco, San Francisco, CA 94143, USA

[7]Lead contact

SUMMARY

Neuron-glia interactions play a critical role in the regulation of synapse formation and circuit assembly. Here we demonstrate that canonical Sonic hedgehog (Shh) pathway signaling in cortical astrocytes acts to coordinate layer-specific synaptic connectivity. We show that the Shh receptor Ptch1 is expressed by cortical astrocytes during development and that Shh signaling is necessary and sufficient to promote the expression of genes involved in regulating synaptic development and layer-enriched astrocyte molecular identity. Loss of Shh in layer V neurons reduces astrocyte complexity and coverage by astrocytic processes in tripartite synapses; conversely, cell-autonomous activation of Shh signaling in astrocytes promotes cortical excitatory synapse formation. Furthermore, Shh-dependent genes *Lrig1* and *Sparc* distinctively contribute to astrocyte morphology and synapse formation. Together, these results suggest that Shh secreted from deep-

This is an open access article under the CC BY-NC-ND license (http://creativecommons.org/licenses/by-nc-nd/4.0/).

*Correspondence: corey.harwell@ucsf.edu.

AUTHOR CONTRIBUTIONS

Conceptualization, Y.X. and C.C.H.; investigation, Y.X., A.T.K., W.W., Z.T.H., O.M., O.O., M.A., S.V., M.K., N.G., D.T., C.C., I.S., and T.E.L.; resources, M.Y.T., W.-C.A.L., B.L.S., and C.C.H.; writing – original draft, Y.X. and C.C.H.; writing – review & editing, Y.X., W.W., A.T.K., M.K., W.-C.A.L., N.G., O.M., O.O., T.E.L., and C.C.H.; funding acquisition, C.C.H.; supervision, C.C.H.

SUPPLEMENTAL INFORMATION

Supplemental information can be found online at https://doi.org/10.1016/j.celrep.2022.110416.

DECLARATION OF INTERESTS

The authors declare no competing interests.

Author Manuscript Author Manuscript Author Manuscript Author Manuscript

layer cortical neurons acts to specialize the molecular and functional features of astrocytes during development to shape circuit assembly and function.

Graphical abstract

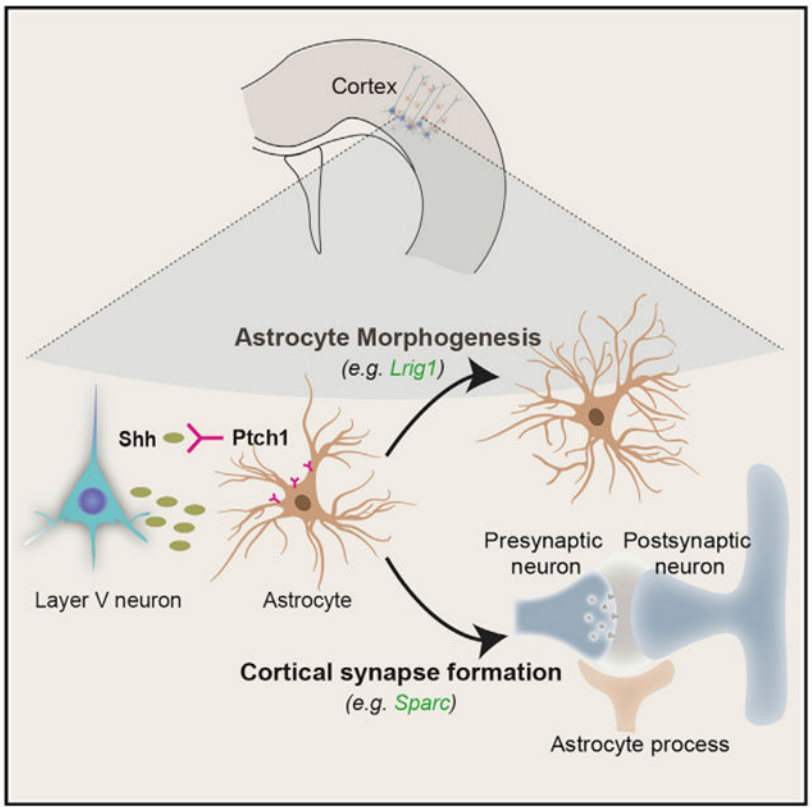

In brief

Xie et al. show that Sonic hedgehog expressed by cortical layer V neurons signals to Ptch1-expressing astrocytes where it is necessary to promote the expression of layer-enriched astrocyte gene networks that control synapse formation and astrocyte morphological complexity.

INTRODUCTION

The mammalian cerebral cortex is organized into six layers composed of neurons that share common projection patterns, molecular identities, and intrinsic physiological properties (Custo Greig et al., 2013). Deep-layer (layers V and VI) cortical projection neurons typically project to a variety of subcortical targets in the brain, while upper-layer (layers II–IV) neurons project to targets within the cortex. The distinctive connection patterns and functional properties of neurons that occupy each cortical layer are essential for the complex circuit computations and behaviors mediated by the cerebral cortex. The extent to which glial cell types which include astrocytes, oligodendrocytes, and microglia also have layer-specific molecular and functional properties to support cortical layer-specific

Author Manuscript Author Manuscript Author Manuscript Author Manuscript

information processing has not been completely determined (Hammond et al., 2019; Marisca et al., 2020; Pestana et al., 2020).

Astrocytes are the most abundant glial cell type in the central nervous system (CNS) and are responsible for supporting a diverse range of functions necessary for cortical circuit activity including neurotransmitter reuptake, ion homeostasis, and synapse formation and elimination (Ben Haim and Rowitch, 2017). It is unclear whether these diverse functions are mediated by a single class of protoplasmic astrocytes or if there are distinct cell subtypes with specialized roles. Recent studies have shown that protoplasmic astrocytes display differences in their morphological and molecular properties that closely correspond to the organization of cortical projection neurons, suggesting the existence of astrocytes with specialized layer-specific functional roles (Batiuk et al., 2020; Bayraktar et al., 2020; Lanjakornsiripan et al., 2018).

How diverse astrocyte subtypes are specified during development is not understood (Akdemir et al., 2020). Fate mapping suggests that cortical astrocytes derived from the same pool of progenitors display tremendous heterogeneity in their location and morphological features (Clavreul et al., 2019). Comprehensive analysis of the molecular diversity of cortical astrocytes has shown that cells with similar molecular features are localized to specific layers (Bayraktar et al., 2020; Lanjakornsiripan et al., 2018). Evidence suggests that neuron-derived cues provide positional information to astrocytes that can regulate specific aspects of their function (Bayraktar et al., 2020; Lanjakornsiripan et al., 2018). The full complement of neuron-derived factors that may regulate the layer-specific molecular identity of astrocytes is currently unknown. Here, we provide evidence that neuron-derived Sonic hedgehog (Shh) is one such factor that is critical to establishing and maintaining layer-specific cortical astrocyte identities.

Shh is most widely known for its role as a morphogen and mitogen during embryonic patterning of the developing nervous system (Garcia et al., 2018; Lee et al., 2016). In the classic model of Shh signaling, the 12-pass transmembrane domain receptor Patched 1 (Ptch1) represses the activity of the 7-transmembrane domain receptor Smoothened (Smo), which is required for activation of Hedgehog signaling. PTCH1 binding to SHH ligand releases the inhibition of SMO, leading to activation of downstream targets such as Gli family transcription factors (Lee et al., 2016). Shh is expressed by subcortical projection neurons in cortical layer V, where it has been shown to regulate the specific patterns of intracortical circuitry (Harwell et al., 2012). Shh signaling is active in a subpopulation of mature astrocytes that are localized primarily to the deep layers of the cortex (Garcia et al., 2010; Hill et al., 2019). In the cerebellum and cortex, Shh signaling in astrocytes promotes the expression of the inward rectifying potassium channel Kir4.1, which is critical for regulating potassium buffering and neuronal excitability (Farmer et al., 2016; Hill et al., 2019). In this study we identify the complement of molecular programs driven by Shh signaling in cortical astrocytes and show that neuron-derived Shh is both necessary and sufficient to promote layer-enriched astrocyte genes involved in regulating synapse formation and function. We show that neuron-derived Shh is required for astrocyte morphogenesis and complete coverage of synapses by perisynaptic astrocyte processes. We analyzed the function of individual Shh-dependent genes and identified distinctive

Author Manuscript Author Manuscript Author Manuscript Author Manuscript

functional roles for *Lrig1* and *Sparc* in regulating astrocyte morphogenesis and cortical synapse formation, respectively. Taken together, our data suggest a model whereby secretion of Shh by layer V cortical projection neurons activates gene expression programs in cortical astrocytes to coordinate their layer-specific morphological and molecular specializations during cortical circuit development.

RESULTS

Expression of the Shh receptor Ptch1 is specific to astrocytes during cortical development

Astrocytes in a number of CNS regions are known to be responsive to Shh signaling (Farmer et al., 2016; Garcia et al., 2010; Hill et al., 2019). The 12-pass transmembrane Shh receptor Ptch1 is known to be required for normal pathway activation during tissue patterning and nervous system development (Rohatgi et al., 2007). To understand the role of Ptch1 in mediating Shh signaling in the developing cortex, we characterized the temporal and cell-type-specific pattern of Ptch1 expression with heterozygous Ptch1-LacZ mutant mice, where a lacZ-neo fusion gene was inserted in the place of the start codon and portions of exon 1 and the entire exon 2 of the *Ptch1* gene (Goodrich et al., 1997). We quantified the density of β-galactosidase-positive (βGal^+) cells in the cortex between postnatal day 5 (P5) and P60 (Figures 1A–1C). At P5, Ptch1-expressing cells were mostly distributed through cortical layers IV to VI. By P15 there was a significant increase in the density of Ptch1-expressing cells in layer I compared with P5 cortex. However, the density of βGal^+ cells was reduced at P28 in layer IV and V, which coincides with the downregulation of neuronal Shh (Figures S1A and S1B). We also observed that the overall density of βGal^+ cells peaks at P60, with layers I to IV accounting for most of the observed increase (Figures 1A–1C). Our data suggest that Ptch1 is dynamically expressed in cortical layers during development and maintains strong expression throughout adulthood.

We further characterized the cell-type identities of Ptch1-expressing cells by immunofluorescence staining for cell-type markers on the cortex of P5–P60 Ptch1-LacZ heterozygous mutant mice (Figures 1D and 1E). At P5, the majority of βGal^+ cells were positive for Olig2, which labels astrocyte and oligodendrocyte precursors at this particular stage. By P15, nearly all βGal^+ cells (96%) were positive for the astrocyte marker S100β while few cells (3.9%) were co-labeled with Olig2. This switch from $Olig2^+$ to $S100\beta^+$ cells at P15 coincides with peak levels of Shh expression (Figures S1A and S1B). The proportion of Ptch1-expressing cell types remained the same until P60 when two populations of βGal^+ cells could be distinguished based upon fluorescence intensity and cell-type marker labeling (Figures S1C and S1D). Low-intensity βGal^+ cells were also positive for the pan-neuron marker NeuN, making up over half of the total βGal^+ population (59%) at this age (Figures 1E, S1C, and S1E). These findings show that Ptch1 is primarily expressed by cortical astrocytes across all layers of the cortex during development, and by P60 it begins to be weakly expressed by subsets of cortical neurons in the mature cortex, suggesting that Shh signaling in the cortex is both cell-type specific and developmental-stage specific.

However, the full complement of genes regulated by activation of Shh signaling in cortical astrocytes is unknown. To address this, we used an astrocyte-specific conditional mutant mouse line in which Shh signaling is hyperactivated by the conditional deletion of Ptch1

Author Manuscript Author Manuscript Author Manuscript Author Manuscript

(Ptch1cKO) (Ferent et al., 2014). To elevate the level of Shh signaling in astrocytes, we crossed GlastCreER mice with two other lines, one carrying a Cre-recombinase conditional allele of Ptch1 and the other an Ai14 reporter line; GlastCreER drives Cre expression specifically in astrocytes, and labels cells with the fluorescent reporter protein tdTomato after tamoxifen administration at P12–P14. We confirmed that inducible loss of Ptch1 expression enhances Shh signaling by examining the expression of Shh signaling pathway components in P21 cortex using RT-PCR. Ptch1 expression was decreased while Shh target genes Smo and Gli1 were increased in Ptch1cKO compared with wild type (WT) (Figure S2A). Using single-molecule fluorescent *in situ* hybridization, we observed increased Gli1 RNA in Ptch1cKO tdTomato$^+$ astrocytes in both upper layer and deep layer (Figures S2B and S2C). Together, our data suggest that inducible loss of Ptch1 is sufficient to activate Shh signaling in cortical astrocytes. Next, we sequenced the transcriptomes of either WT or Ptch1cKO fluorescence-activated cell sorting (FACS)-purified tdTomato$^+$ cortical astrocytes to assess differential gene expression in response to increased levels of Shh signaling (Figures 1F and S2D–S2G).

We observed 77 upregulated and 91 downregulated genes in Ptch1cKO astrocytes using $|\log_2\text{FoldChange}| > 1$ and $p < 0.01$ cutoffs (Figures S2I and S2J). Shh pathway genes *Smo* and *Hhip* were significantly increased whereas there was a 40% reduction of *Ptch1* transcripts in Ptch1cKO compared with WT, suggesting efficient tamoxifen-induced recombination (Figure S2H). Upregulated genes in Ptch1cKO astrocytes were involved in processes related to cell localization, immune system, and cell metabolism, while downregulated genes in Ptch1cKO astrocytes were enriched for gene ontology terms related to nervous system development (Figures S2K and S2L). Genes that were significantly increased in Ptch1cKO included *Kir4.1/Kcnj10, Kir5.1/Kcnj16* (inward rectifying potassium channel), *Lrig1* (leucine-rich repeats and immunoglobulin-like domains 1), *Il33* (cytokine interleukin-33), and *Sparc* (secreted protein acidic and rich in cysteine) (Figure 1G). Many of these genes have been shown to be enriched in astrocytes and important factors regulating synapse formation and function (Alsina et al., 2016; Jones et al., 2018; Kucukdereli et al., 2011; Vainchtein et al., 2018). A number of genes downregulated in Ptch1cKO astrocytes (Figure 1G) have been shown to be enriched in astrocytes (Mazare et al., 2020; Morte and Bernal, 2014; Zhang et al., 2014; Zhao and Gammie, 2015). Together, these data suggest that loss of Ptch1 in cortical astrocytes promotes the expression of genes involved in astrocyte-mediated synapse development and circuit function.

Loss of Ptch1 in cortical astrocytes is sufficient to promote the expression of layer-enriched genes

Given their potential roles in astrocyte-mediated synapse development, we chose to focus on genes that were upregulated in Ptch1cKO to determine whether their increases were equivalent across all cortical layers. We used RT-PCR and fluorescent *in situ* hybridization to verify the increased expression of *Kir4.1, Lrig1, Sparc,* and *Il33* in Ptch1cKO mice and found that all of these genes were significantly increased in cortical astrocytes (Figures 2D, 2H, 2L, 2P, S4A, and S4B), confirming our RNA-sequencing (RNA-seq) analysis (Figures 2C, 2G, 2K, and 2O).

Author Manuscript Author Manuscript Author Manuscript Author Manuscript

Previous work has shown that Kir4.1 is expressed exclusively in glial cells in the CNS and is thought to be required for potassium buffering in the brain (Djukic et al., 2007; Tong et al., 2014). We found that Kir4.1 expression was highly enriched in cortical layer IV and layer Vb WT astrocytes, which extensively overlaps with the location of Shh-expressing neurons (Figures 2A and S1A). In Ptch1cKO mice, Kir4.1 fluorescence intensity was dramatically increased across all layers compared with WT (Figures 2A and 2B), suggesting that astrocytes across all layers of the cortex have a similar capacity to respond to Shh signaling. We measured the fluorescence intensity of Kir4.1 of individual WT and Ptch1cKO tdTomato$^+$ astrocytes and found that Kir4.1 signal was significantly increased in Ptch1cKO astrocytes (Figure S3B); however, the proportion of Kir4.1$^+$Sox9$^+$ astrocytes was not changed in Ptch1 mutants (Figure S3A). Moreover, the total number of astrocytes remained stable in Ptch1cKO mice (Figures S4C and S4D). Taken together, these data suggest that Shh signaling increases the levels of Kir4.1 but not the number of Kir4.1-expressing astrocytes. We also observed increased expression of Kir5.1, a pH-sensitive inward rectifying potassium channel that is capable of forming heteromeric complexes with Kir4.1 (Brasko et al., 2017) (Figures S4E–S4G). Next, we verified whether the expression of Lrig1, Il33, and Sparc was increased in response to Ptch1 loss of function. In WT animals, we observed that Lrig1 was most highly expressed in layer IV, largely overlapping with tdTomato$^+$ astrocytes at P21 (Figure 2E), while Il33 was predominantly expressed in deep-layer astrocytes (Figure 2I), consistent with previous analyses (Bayraktar et al., 2020). Sparc$^+$ cells were evenly distributed in between upper and deep layers (Figure S4H) and were found in both tdTomato$^+$ astrocytes (Figure 2M) and Iba1$^+$ microglia cells (Figure S4I). As expected, we observed that the density of Lrig1$^+$, Il33$^+$, and Sparc$^+$ cells was significantly increased throughout upper and deep layers of Ptch1cKO cortex (Figures 2E, 2F, 2I, 2J, 2M, and 2N). In contrast to Kir4.1, Shh signaling appears increase both the level and the number of astrocytes expressing these target genes (Figures S3C–S3H). Notably, we did not observe an increase in the density of Sparc$^+$Iba1$^+$ cells in Ptch1cKO (Figures S4I and S4J), confirming that the changes in Sparc expression are confined to astrocytes. Taken together, our findings indicate that loss of Ptch1 is sufficient to promote the expression of layer-enriched genes in cortical astrocytes during development.

Sonic signaling is necessary for layer-enriched astrocyte molecular features

To test whether layer V neuron-derived Shh was specifically required to maintain the expression of target genes in cortical astrocytes, we specifically deleted Shh in the cortex by crossing the Emx1 *ires*-cre mice with a line carrying a conditional *Shh* deletion allele (Shhflox/flox) (Harwell et al., 2012). We confirmed the loss of cortical Shh in Emx1Cre;Shhflox/flox (ShhcKO) mice by examining Shh signaling components, including transcriptional targets Gli1 and Ptch1. The expression of Ptch1, Gli1, and Shh were significantly decreased in ShhcKO cortex compared with Shhflox/flox (WT) (Figure S5A), additionally, Gli1 transcripts were dramatically decreased in deep layers of the cortex where they are typically enriched (Figures S5B and S5C). Next, we analyzed the abundance and distribution of Kir4.1 in the cortex using immunohistochemistry and RT-PCR in P21 WT and ShhcKO mice. Kir4.1 expression was significantly decreased in layers IV and Vb of ShhcKO mice at P21 (Figures 3A–3C). This is consistent with previously reported observations whereby disrupted Shh signaling by deletion of the Shh receptor Smo led

Author Manuscript Author Manuscript Author Manuscript Author Manuscript

to reduced Kir4.1 expression (Farmer et al., 2016; Hill et al., 2019). To investigate whether Kir5.1 was also decreased in ShhcKO cortical neurons, we used single-molecule fluorescent *in situ* hybridization to detect *Kir5.1* transcripts and observed a similar pattern of significantly reduced *Kir5.1* expression in the deep layers of cortex (Figures S5D and S5E).

We also detected significant reductions of both protein and RNA for the layer-enriched astrocyte genes *Lrig1* and *Il33* (Figures 3D–3I and S5F), as well as a non-layer-enriched gene *Sparc,* in the cortex of ShhcKO mice (Figures 3J–3L). Surprisingly, the number of $Il33^+$ cells was comparable with control levels in both upper and deep layers of adult ShhcKO mice (Figures S5G and S5H). Previous research has shown that in the adult mouse CNS, Il33 is mainly expressed by oligodendrocytes (Gadani et al., 2015). We immunostained the cortex of 4-month-old WT mice for Il33 and the oligodendrocyte marker Olig2 and found that Il33 was primarily enriched in $Olig2^+$ cells (Figure S5I). Thus, the expression pattern of Il33 appeared to shift from Shh-signaling-dependent astrocyte-specific to Shh-independent oligodendrocyte-specific expression over the course of development. Collectively, these data suggest that secretion of Shh by layer V cortical neurons is required to maintain a complement of layer-enriched astrocyte genes during development.

Neuron-derived Shh is sufficient to promote deep-layer astrocyte molecular identity

Recent studies have shown that the morphological and molecular differences between cortical astrocytes are driven by neuronal layers (Bayraktar et al., 2020; Lanjakornsiripan et al., 2018). To determine whether a neuron-specific source of Shh is sufficient to induce astrocytes to adopt a deep-layer astrocyte molecular profile, we misexpressed a full-length Shh transgene in upper-layer neurons, where it is typically absent. We co-electroporated plasmids encoding pCAG-IRES-Cre and Flex-Shh-IRES-GFP into the lateral ventricles of embryonic day 15 (E15) mouse embryos, a period when the majority of cortical progenitors generates upper-layer neurons (Figure 4A). Plasmids encoding pCAG-IRES-Cre and Flex-tdTomato were used as controls. Brains were collected at P14 and stained for Kir4.1, Lrig1, Il33, and Sparc. We did not observe any differences in the survival or migration of upper-layer neurons overexpressing Shh compared with electroporations with control plasmids. Compared with the non-electroporated contralateral side and control plasmid electroporations, astrocyte-specific target gene expression was increased in upper-layer cortical astrocytes in proximity to the somatodendritic region of neurons overexpressing Shh (Figures 4B–4I). These results suggest that SHH can be released from the somatodendritic region of neurons and is sufficient to promote deep-layer astrocyte transcriptional programs in the developing cortex.

Shh signaling is required for astrocyte morphogenesis and coverage of neuronal synapses

Protoplasmic astrocytes have complex arbors containing fine cellular processes that infiltrate in the neuropil and interact with synapses (Allen and Eroglu, 2017; Bushong et al., 2002). Astrocytes that occupy different cortical layers exhibit diverse morphological features (Lanjakornsiripan et al., 2018). We investigated whether neuron-derived Shh expression is required for astrocytes to acquire their unique morphological properties. We utilized postnatal astrocyte labeling by electroporation (PALE) (Stogsdill et al., 2017) with a plasmid

Author Manuscript Author Manuscript Author Manuscript Author Manuscript

encoding membrane *tdTomato* and nuclear GFP (pCAG-mTdT-2A-H2BGFP) to sparsely label astrocytes across the entire cortex of WT and ShhcKO mice (Figures 5A and 5B). Sholl analysis of fluorescent labeled astrocytes showed that morphological complexity of deep-layer astrocytes is significantly reduced in ShhcKO mice compared with controls, whereas we observed no change in upper-layer astrocytes (Figures 5C and 5D). Loss of cortical Shh did not lead to a reduction in the number or altered distribution of S100β$^+$ astrocytes (Figures S6A and S6B). We next tested whether activation of Shh in cortical astrocytes might promote increased morphological complexity in tdTomato$^+$ Ptch1cKO astrocytes when compared with control labeled cells. We did not observe significant differences in morphological complexity between Ptch1cKO and controls (Figures S6C and S6D). Taken together, our data suggest that Shh signaling is necessary to maintain the morphological properties of deep-layer astrocytes *in vivo*.

We next used electron microscopy (EM) to test the possibility that reduced morphological complexity of ShhcKO astrocytes might lead to reduced formation of perisynaptic astrocyte processes (Araque et al., 1999). We generated EM image volumes (Graham et al., 2019) spanning all six layers of the somatosensory cortex of P26–P28 WT and ShhcKO animals (Figure 5E) and quantified structural features of synapses. We traced 2,244 synapses and their associated astrocyte processes (456 WT layer V, 496 KO layer V, 636 WT layer II, 656 KO layer II) across 20 well-aligned serial sections. Three-dimensional reconstructed images from WT and ShhcKO showed astrocyte processes surrounding synapses at the level of the synaptic cleft (Figure S6E). We did not detect a change in the density of tripartite synapses in either layer II or layer V of ShhcKO cortex compared with controls (Figures 5F and 5G) or a change in the density of neuronal synapses (Figures S6F and S6G). We also did not observe a change in the proportion of synapses that were associated with astrocyte processes (Figures 5H and 5I). We further investigated whether Shh signaling might influence the structure of perisynaptic astrocyte processes by measuring the extent of ensheathment of synaptic clefts by astrocytes in layer II and layer V. Intriguingly, the fraction of synaptic interface perimeter that was surrounded by perisynaptic astroglia in both layer II and layer V KO were significantly reduced compared with WT (Figures 5J and 5K; Table S1), suggesting that astrocytes in ShhcKO have less structural connection with surrounding deep-layer neurons. We also observed more astrocytes with intensely labeled glycogen granules accumulated in their processes and increased density of GFAP$^+$ astrocytes in all cortical layers of ShhcKOs (Figures 5J, 5L, and S6H–S6J; Table S2). These observations suggest that astrocytes become reactive when neuronal Shh is deleted (Cai et al., 2020; Cali et al., 2019b; Dienel and Rothman, 2019; Allahyari et al., 2019). Together, our data suggest that Shh signaling in the cortex is necessary for astrocyte morphogenesis and proper formation of astrocyte-neuron structural connections.

Loss of Ptch1 in astrocytes promotes cortical synapse formation

Astrocytes are viewed as integral elements of excitatory synaptogenesis, and our molecular analysis suggests that Shh signaling promotes the expression of genes involved in synaptic function (Baldwin and Eroglu, 2017). To determine whether activation of Shh signaling in astrocytes might function to promote synaptogenesis, we quantified the synapse density within WT and Ptch1cKO tdTomato$^+$ astrocyte territories. Synapses were labeled by the

Author Manuscript Author Manuscript Author Manuscript Author Manuscript

co-localization of pre- and postsynaptic markers VGluT1/PSD95 (V1) and VGluT2/PSD95 (V2), which represent cortical excitatory and thalamocortical excitatory inputs, respectively. We found that the density of both V1 and V2 co-localized puncta was significantly increased within Ptch1cKO astrocyte domains in both layer II and layer V (Figures 6A–6D and S7A). However, deletion of Shh decreased the density of V2 co-localized puncta in deep-layer PALE territory but did not significantly reduce the density of V1 co-localized puncta (Figures S7B and S7C). This could be attributable to the diversity of VGluT1^{+} corticocortical inputs and their capacity to compensate for Shh-dependent connections.

We asked whether increased glutamatergic synapses in Ptch1cKO leads to changes in functional connections by examining spontaneous miniature excitatory postsynaptic currents (mEPSCs) in layer V pyramidal neurons in acute brain slices. The frequency of spontaneous mEPSCs in layer V neurons was increased (35.75%) in Ptch1cKO slices compared with WT, while there was no change in mEPSC amplitude, input resistance, or membrane capacitance (Figures 6E–6G, S7D, and S7E). To further determine whether cell-autonomous activation of Shh signaling in cortical astrocytes promotes layer II to layer V connectivity, we examined the evoked EPSCs in layer V pyramidal neurons, which was induced by a serial electrical stimulation of layer II neurons. Layer V neurons in Ptch1cKO showed significantly increased EPSC amplitude in response to layer II stimulation (Figure 6H). Taken together, our data suggest that astrocyte-specific activation of Shh signaling through loss of Ptch1 promotes the formation of glutamatergic synapses and enhances the strength of layer II to layer V connections.

Shh target genes *Lrig1* and *Sparc* distinctively contribute to astrocyte morphogenesis and synapse formation

To determine whether specific Shh target genes may have prominent roles in regulating astrocyte morphogenesis or synapse formation, we selected three candidate genes for further analysis: *Il33, Sparc,* and *Lrig1*. Indeed, Il33 and Sparc have been previously implicated in regulating astrocyte-mediated synaptic development in the CNS, although none of these genes has been extensively studied in the developing cerebral cortex (Jones et al., 2011, 2018; Kucukdereli et al., 2011; Vainchtein et al., 2018). Even though Lrig1 function has not been evaluated in astrocytes, recent studies have shown that Lrig1 regulates neural precursor cell proliferation and hippocampal neuron dendrite arborization (Alsina et al., 2016; Jeong et al., 2020). We therefore investigated whether knockdown of these genes might regulate astrocyte morphogenesis and synapse formation. We co-electroporated P0–P1 mice with pCAG-mTdT and CMV-tGFP-shRNAs targeting either Il33, Sparc, Lrig1, or scramble short hairpin RNA (scr-shRNA) controls (Figure 7A). Nearly all tdTomato fluorescent cells co-expressed GFP at 3 days post injection (Figure S8A), indicating efficient co-electroporation with both plasmids. To further confirm the shRNA effectiveness, we delivered Lrig1-shRNA into cortical progenitor cultures, which have highly enriched lrig1 expression (Jeong et al., 2020) (Figure S8B), and validated Sparc and Il33 knockdown efficiency in astrocyte cultures and *in vivo* where each hairpin produced significant reductions in transcripts and proteins of their target genes (Figures S8C–S8E). Next, we investigated whether knockdown of those genes regulates the morphological complexity of deep-layer tdTomato^{+} astrocytes. Lrig1-shRNA knockdown astrocytes exhibited significantly reduced morphological complexity

Author Manuscript Author Manuscript Author Manuscript Author Manuscript

compared with scr-shRNA (Figures 7B and 7C), and there was also a modest decrease in the morphological complexity of Sparc-shRNA astrocytes (Figures S8F and S8G). Surprisingly, we observed increased complexity of the most distal processes of Il33-shRNA astrocytes (Figures S8F and S8H). This observation may be relevant to previously described functions of Il33 related to synapse pruning or immune function (Gadani et al., 2015; Vainchtein et al., 2018). Next, we tested whether any of these three genes is necessary for astrocyte-mediated excitatory cortical synapse formation. We stained for both VGluT1/PSD95 (V1) and VGluT2/PSD95 (V2) in shRNA knockdown astrocytes, followed by analysis of co-localized puncta in astrocyte territories. We observed a significant decrease in the density of V1 co-localized puncta in deep-layer Sparc knockdown astrocytes (Figures 7D and 7F), with no significant differences in Lrig1 and Il33 shRNA groups compared with controls (Figures 7F, S8I, and S8K). However, the density of the V2 co-localized puncta was not changed in Sparc knockdown astrocytes (Figures 7E, 7G, S8J, and S8L), suggesting that Shh-dependent Sparc in cortical astrocytes may be prominently involved in regulating VGluT1 cortical synapse formation. This loss of VGluT1 synapses in Sparc knockdown astrocytes contrasts with the loss of VGluT2 observed in ShhcKO (Figure S7C). These observations suggest that loss of an individual Shh target gene may have different impacts on synapse formation when compared with the combinatorial reduction of a network of genes in ShhcKO. Taken together, our data suggest that individual target genes significantly contribute to distinctive aspects of Shh-dependent astrocyte functions, with Lrig1 being important for astrocyte morphogenesis, while Sparc is essential for promoting cortical synapse formation. Thus, the combinatorial contribution of target genes is necessary for the diverse repertoire of Shh-dependent astrocyte behaviors during cortical development.

DISCUSSION

Shh signaling regulates the expression of a diverse repertoire of deep-layer astrocyte-enriched target genes with known roles in regulating various aspects of synaptic transmission including synapse formation (*Sparc, Hevin/Sparcl1, Lrig1*) (Alsina et al., 2016; Jones et al., 2011; Singh et al., 2016), refinement (*Il33*) (Vainchtein et al., 2018), ion homeostasis, and neurotransmitter uptake (*Kir4.1/Kcnj10 and Kir5.1/Kcnj16*) (Brasko et al., 2017; Djukic et al., 2007). The diversity of molecular functions of Shh target genes suggests that signaling shapes multiple aspects of astrocyte development and function, impacting morphology, the secretion of synaptogenic factors, and cellular adhesions (Allen and Eroglu, 2017).

Our data are consistent with previous studies showing that Sparc promotes the number of GluA1-containing AMPARs at synapses and enhanced synaptic function (Jones et al., 2018). However, this interpretation contrasts with other studies suggesting that Sparc functions as a negative regulator of synapse formation (Kucukdereli et al., 2011) ora “molecular brake” preventing the accumulation of GluA1 at developing synapses (Jones et al., 2011). However, it is worth noting that the analyses that led to these conclusions were primarily carried out using a null mutant mouse line where Sparc is deleted in both astrocytes and microglia, while our Sparc knockdown experiments were restricted to astrocytes. As discussed further below, experimental approaches that define the cell-specific roles of genes such as Sparc will be necessary to gain a clearer picture of their context-dependent function.

Author Manuscript Author Manuscript Author Manuscript Author Manuscript

Previous studies have shown that both *Sparc* and *Lrig1* have Gli-binding regions in embryonic stem cell-derived neural progenitors (Peterson et al., 2012), indicating a potential mechanism by which these genes are directly regulated by Shh signaling in cortical astrocytes. Studies to determine the mechanisms by which these Shh target genes promote synapse formation and astrocyte maturation should provide insight into the key molecular pathways orchestrating complex cellular behaviors and interactions during cortical circuit development.

In our data analysis we demonstrate that astrocyte-specific activation of Shh signaling is sufficient to promote synapse formation. An intriguing question for future study is whether Shh signaling in neurons and astrocytes regulates the formation of specific types of synaptic inputs. In our EM analysis we find no alteration in synapse density in ShhcKOs. However, when we examined the type of glutamatergic synapses with immunohistochemistry, we observed a specific reduction of deep-layer VGluT2 synapses in ShhcKO. This contrasts with Ptch1cKO where both VGluT2 and VGluT1 synapses were increased. Based upon our current data and our previous findings (Harwell et al., 2012), we could speculate that Shh signaling is required for all types of VGluT2 synapses but only a subset of VGluT1 synapses. While Shh-dependent VGluT1 synapses are lost, their reduction could be compensated by a subset of Shh-independent VGluT1 inputs. In the future, it will be necessary to identify the specific neuronal inputs that are gained or lost in response to changes in Shh signaling.

Our data show that Shh signaling controls both the layer-specific gross morphological complexity of cortical astrocytes and coverage of synapses by their fine processes. Not all cortical synapses are ensheathed by astrocytes, and the mechanisms that determine the types of synapses and the extent of synapse ensheathment are not known. We found that the extent of the physical interaction with synapses is dependent upon Shh signaling while the number of perisynaptic astrocyte processes is unchanged. This suggests that establishment of perisynaptic astrocyte processes and the extent of their growth may be two distinctive processes. It is also possible that gross morphological complexity of astrocytes is correlated with their connection with synapses such that less complex astrocytes might lead to reduced coverage of surrounding synapses. In addition to the known astrocyte-neuron interactions, astrocytes also tightly wrap blood vessels through their elaborate perivascular endfeet (Abbott et al., 2006). Loss of astrocyte complexity through reduced Shh signaling might also have an impact on the blood-brain barrier (BBB) function, as previous reports have suggested a connection between Shh signaling and BBB integrity (Alvarez et al., 2011). In future studies it will be important to determine whether astrocyte interactions with other non-neuronal cell types are Shh dependent.

Il33 undergoes two phases of expression: first an Shh-dependent, astrocyte-specific phase in the developing cortex and then an Shh-independent, oligodendrocyte-specific phase in the mature cortex (Figures 3 and 5I). Oligodendrocyte-specific Il33 has been shown to be required for oligodendrocyte maturation (Sung et al., 2019), while its expression in astrocytes was shown to regulate microglial synapse pruning (Vainchtein et al., 2018). This finding highlights the importance of accounting for the cell type and developmental stage-specific expression patterns of Shh target genes when interrogating their function.

Author Manuscript Author Manuscript Author Manuscript Author Manuscript

Indeed, both Il33 and Sparc are known to be expressed by other glial cells in the developing brain, but it is only the astrocyte-specific expression of these genes that is regulated by Shh signaling.

During embryonic development, SHH is thought to disperse from floor plate cells to form a gradient that specifies cell types along the dorsoventral axis of the developing CNS (Dessaud et al., 2008). It is not known whether similar mechanisms are at play to release SHH from the morphologically complex and polarized neurons in the cortex. Research on the developing limb bud suggests that SHH may be trafficked over long distances in cytonemes (Sanders et al., 2013). A similar trafficking mechanism in neurons would provide an intriguing means for controlling the delivery of SHH to local astrocytes. Many Shh target genes including *Gli1, Kir4.1, Il33,* and *Lrig1* have sharp boundaries of expression that demarcate neuronal layers Va and Vb (Figures 2 and 3). Our data are consistent with others suggesting that least some portion of SHH protein is released by the somatodendritic compartments of cortical projection neurons (Rivell et al., 2019). When Shh was either deleted or overexpressed, the most robust gene expression changes were observed in the astrocytes located in close proximity to neuron cell bodies (Figures 3 and 4). Future studies focused on understanding the mechanisms that regulate the trafficking, sequestration, and release of SHH protein in neurons will provide important insights into mechanisms of how neurons communicate with their astrocyte neighbors.

Peak expression of Shh coincides with the peak period of cortical synaptogenesis in mouse (Farhy-Tselnicker and Allen, 2018). However, the Shh receptors Ptch1 and bioregional Cdon-binding protein (Boc) both maintain a high level of expression throughout adulthood (Figures 1A–1C). Boc remains exclusively expressed in neurons throughout development and adulthood (Harwell et al., 2012), while Ptch1 is initially exclusive to cortical astrocytes lineages and then begins to be expressed in adult neurons (Figure S1C). The functional relevance of Ptch1 expression in adult cortical neurons has yet to be explored. One intriguing possibility is that cell-type- and layer-specific responses to Shh signaling in the cortex may be further diversified by combinatorial expression of Shh receptors and interacting proteins. It is possible that Shh signaling in neurons and astrocytes during development is required to establish cortical circuitry, while signaling in the adult cortex may have roles in synaptic maintenance or plasticity. The respective neuron- and astrocyte-specific expression of Boc and Ptch1 during cortical development suggests a model whereby layer Vb neuron-derived Shh signals to intracortical projection neurons through Boc and to astrocytes through Ptch1. Evidence from previous research has shown that different downstream signaling pathways are activated through these receptors, with Ptch1 being required for transcriptional regulation of Gli1 while Boc is necessary for Src family kinase signaling (Yam et al., 2009). There are also instances in which Boc and Ptch1 have been shown to function cooperatively in *cis* (Allen et al., 2011; Izzi et al., 2011). Future studies are necessary to determine whether *trans* interactions between these receptors allow Shh to function as a layer-specific organizer that coordinates both neurons and astrocytes to facilitate synaptic development.

Author Manuscript Author Manuscript Author Manuscript Author Manuscript

Limitations of the study

We believe our work here complements, contrasts, and extends the work published by Hill et al. (2019); however, our models differ in very important ways, Hill et al. disrupt Shh signaling in astrocytes by knocking out the Shh receptor Smoothened which leads to increased excitability and increased synapses on apical dendrites, suggesting that loss of Shh signaling astrocytes functions to promote synapse formation. Our model is based upon the observations that glutamatergic synapses are decreased upon loss of cortical neuron-derived Shh and the complementary observation that increased Shh signaling in astrocytes from Ptch1 deletion promotes cortical synapse formation through the specific network of genes that we identified with our RNA-seq analysis. The contrasting model derived from our study suggests that disrupting Shh signaling in astrocytes through non-autonomous deletion of neuron-derived Shh ligand versus cell-autonomous deletion of the Shh receptor Smo may have drastically different impacts on synapse formation. It is important to consider that deletion of Shh ligand in the cortex will impact signaling in both Ptch1-expressing astrocytes and Boc-expressing intracortical neurons, whereas Hill et al. specifically targeted Smo-expressing astrocytes. In future studies, it will be necessary to determine how Smo deletion in astrocytes affects Shh ligand levels and signaling in Boc-expressing cortical neurons.

STAR★METHODS

RESOURCE AVAILABILITY

Lead contact—Further information and requests for resources and reagents should be directed to and will be fulfilled by the lead contact, Corey Harwell (corey.harwell@ucsf.edu).

Materials availability—This study did not generate new unique reagents.

Data and code availability

- RNA-seq data have been deposited at GEO and are publicly available as of the date of publication. Accession numbers are listed in the key resources table. Microscopy data reported in this paper will be shared by the lead contact upon request.
- All original code has been deposited at Zenodo and is publicly available as of the date of publication. DOIs are listed in the key resources table.
- Any additional information required to reanalyze the data reported in this paper is available from the lead contact upon request.

EXPERIMENTAL MODEL AND SUBJECT DETAILS

All animal procedures conducted in this study followed experimental protocols approved by the Institutional Animal Care and Use Committee of Harvard Medical School. Mouse lines are listed in the key resources table. Mouse housing and husbandry conditions were performed in accordance with the standards of the Harvard Medical School Center of Comparative Medicine. Embryonic (E) day 13 and Postnatal (P) day 1-120 mice were used

Author Manuscript Author Manuscript Author Manuscript Author Manuscript

for this study. The postnatal mouse ages for each experiment are indicated in figures and figure legends. For all mouse studies the sex of postnatal mice and primary cell culture tissue were not determined. All cells were cultured in standard cell culture medium in 37°C with 5% CO2.

METHOD DETAILS

Tamoxifen administration—Tamoxifen (Sigma) was dissolved in corn oil at a concentration of 20 mg/ml at 37°C and stored at 4°C for the duration of injections. For P12 mice (WT: Glast-CreER^{T2}; Ai14 or Ptch1cKO: Glast-CreER^{T2}; Ptch1$^{flox/flox}$; Ai14), 10-15 μL of tamoxifen was injected intraperitoneally for three consecutive days in order to induce effective recombination. For Shh-CreER^{T2}; Ai14 mice, the dose of tamoxifen varied with mouse weight (age). Mice were closely monitored for any adverse reactions to the treatment.

Immunofluorescence staining—Postnatal animals were transcardially perfused with PBS followed by 4% paraformaldehyde (PFA), their brains were dissected out and post-fixed in 4% PFA overnight at 4°C. Brains were sliced into 50 μm sections on a vibratome (Leica Microsystems VT1200S). Sections were prepared and placed in blocking solution (0.3% Triton (Amresco), and 10% goat serum) for 1-2 h at room temperature. After washing with PBS, sections were incubated sequentially with primary antibodies overnight at 4°C and secondary antibodies for 1 h at room temperature (RT). DAPI (4',6-diamidino-phenylindole, Invitrogen) was added to the secondary antibodies solution. The sections were mounted using ProLong Gold Antifade Mountant (Invitrogen). Cryosections: Brains were cryoprotected in 30% sucrose/PBS overnight at 4°C after post-fixation. Brains were embedded in O.C.T. compound (Sakura), frozen on dry ice and stored at −80°C. Samples were sectioned at 20 μm on a cryostat (ThermoFisher CryoStart NX70). Images were acquired using a Leica SP8 laser point scanning confocal microscope, 10X, 20X, 40X, 63X and 100X objectives were used and images were further analyzed using Fiji, brightness and contrast were adjusted as necessary for visualization, but the source images were kept unmodified.

***In situ* hybridization (RNAscope)—**Fresh frozen brain sections were prepared and pretreated by using the RNAscope fluorescent multiplex assay. RNA probes (see key resources table) against *Lrig1*, *Kir5.1* were combined with a probe against an astrocyte marker *Aldh1l1*, for Ptch1cKO samples, multiplex RNAscope was done by combining *Lrig1, Kir5.1* and *Gli1* probes with a *tdTomato* probe to confirm that labeled cells are recombined cells.

Electron microscopy—Sample preparation: mice were transcardially perfused with Ames' medium (oxygenated with 95% O_2, 5% CO_2, warmed to 37°C) to remove blood, and then a fixative solution (2.5% glutaraldehyde (Electron Microscopy Sciences) and 2% paraformaldehyde (Sigma) in cacodylate buffer (0.1 M sodium cacodylate (Electron Microscopy Sciences), pH 7.4 and 0.04% $CaCl_2$ (Sigma), warmed to 37°C). Brains were dissected out and then post-fixed in the same fixative at 4°C overnight. After washing the samples with cacodylate buffer, brains were sectioned to 200 μm thickness using a

Author Manuscript Author Manuscript Author Manuscript Author Manuscript

vibratome, then stored in 3% glutaraldehyde in cacodylate buffer at 4°C before heavy metal staining. Heavy metal staining: sections were washed with cacodylate buffer. Then trimmed to include on the regions of interest (somatosensory cortex). Samples were then stained in 1% osmium tetroxide aqueous solution (Electron Microscopy Sciences) with 2.5% potassium ferrocyanide (MilliporeSigma) at RT for 1h. Sections were rinsed in water and then maleate buffer (MilliporeSigma) (pH=6.0) and stained in 0.05 M Maleate Buffer containing 1% uranyl acetate (Electron Microscopy Sciences) at 4°C overnight. Embedding: Sections were dehydrated in series of washes from 5% to 100% ethanol, then infiltrated with 1:1 Epon resin: propylene oxide at 4°C for overnight. Finally, sections were embedded in 100% Epon resin and polymerized at 60°C for 48–72 h. Serial sectioning and EM imaging: serial ultrathin sections (40-50 nm thick, 100-250 sections) were collected and imaged using the automated TEMCA-GT pipeline (Maniates-Selvin et al., 2020). Images were collected at 2500x magnification resulting in 4.3 nm pixels. Images were elastically aligned to form a 3D image volume using AlignTK software (see key resources table) run on the O2 computing cluster at Harvard Medical School. Image analysis: Image volumes were accessed and annotated using the CATMAID software (see key resources table). All synapses and astrocytes within regions of interest of layer II and layer Vb of P26-P28 WT and ShhcKO samples (three random regions were chosen, each area size is 20×10×0.9 μm, axes correspond to medial-lateral, dorsal-ventral, and anterior-posterior directions, respectively) were annotated. Volumes representative of layer II and layer V were chosen at the same respective distance from the corpus callosum in both WT and ShhcKO samples. Synapses were identified by their characteristic structural features, namely synaptic vesicles in the presynaptic compartments along with darkly stained postsynaptic densities. Astrocyte processes were distinguished by their irregular shape and dense glycogen granules (Cali et al., 2019a; Kikuchi et al., 2020). For each synapse, the area of the post-synaptic density (PSD) was traced. Synapses whose cleft was surrounded by astrocytic processes were also labeled as astroglia synapses. For 3D visualization of synapses, image data surrounding the synapse was extracted using the pymaid API (https://pymaid.readthedocs.io/en/latest/), then manually segmented using itk-SNAP (see key resources table). Only a few representative astroglia synapses were reconstructed this way. Astrocyte contact fraction analysis: astrocytic perimeter was measured by summing the length of the astrocyte contacts at the edges of synaptic axon-dendrite interface. And the total perimeter was measured by summing the astrocyte contact length and the edges of axon-dendrite, then the fraction of astrocytic contact was determined. Glycogen granules analysis: a single cross-section of each tripartite synapse with a prominent PSD was manually segmented using itk-SNAP. Astrocytic glycogen granules were identified as dark, round spots, 50-80 nm in diameter, that were distributed over a relatively clear cytoplasm.

RNA-Seq—Brains were dissected out after transcardial perfusion of animals with PBS and sliced into coronal sections with a 1.0 mm brains slicer Matrix (BSMAS001-1). A 1 mm X 2 mm piece of somatosensory cortex was cut off and minced tissues into small pieces. Cortical tissues were digested with accutase (ThermoFisher) on a rotator at 4°C. Cells were centifuged at 2000 rpm for 2 min at 4°C. The cell pellet was resuspended in ice cold Hibernate-A (ThermoFisher) and triturated with a 1 ml pipette tip until the cortical chunks disappeared. The cell suspension was gently pipetted out through a 70

Author Manuscript Author Manuscript Author Manuscript Author Manuscript

μm filter, and ~800K cells were sorted by tdTomato fluorescence, tdTomato– cells were sorted out as well to use as negative controls. RNA was then purified with a RNeasy Mini Kit (Qiagen). The concentration and quality of purified RNA were determined using BioAnalyzer (Agilent), and the RNA was reverse-transcribed into cDNA and amplified by RNA-based single primer isothermal amplification (SPIA) using the Ovation RNA-seq system V2 (NuGEN). Synthesized cDNA was sonicated using a Covaris S2 ultrasonicator to reduce the fragment size range to 100-600 bp. 100 ng of sheared cDNA were end paired, ligated with barcoded adaptors, amplified and purified using the Ovation Ultralow System V2 (NuGEN). RNA Exome Capture and Sequencing: targeted exome hybrid capture was performed using Illumina TruSeq Exome Capture reagents according to manufacturer's protocol on a Beckman Coulter Biomek FX. Post capture the library pools were quantified by Qubit fluorometer, Agilent TapeStation 2200, and RT-qPCR using the Kapa Biosystems library quantification kit according to manufacturer's protocols. Uniquely indexed libraries were pooled in equimolar ratios and sequenced on an Illumina NextSeq 500 with single-end 75bp reads by the Dana-Farber Cancer Institute Molecular Biology Core Facilities. Libraries were sequenced in an Illumina NextSeq 500 to a sequencing depth of 28-40 million reads per sample.

RNA-seq Analysis—Sequenced reads were aligned to the UCSC mm10 reference genome assembly and gene counts were quantified using STAR (v2.5.1b) (Dobin et al., 2013). Differential gene expression testing was performed by DESeq2 (v1.10.1) (Love et al., 2014) and normalized read counts (FPKM) were calculated using cufflinks (v2.2.1) (Trapnell et al., 2010). RNAseq analysis was performed using the VIPER snakemake pipeline (Cornwell et al., 2018). Significant genes were identified using a threshold of $P<0.05$, Lists of differentially expressed genes were examined by gProfiler for statistical enrichment of information such as Gene Ontology (GO) terms, biological pathways functional redundancy in over-represented GO terms identified by gProfiler was reduced with REVIGO for a visual representation of the most prominent processes.

Quantitative reverse transcriptase polymerase chain reaction (qRT-PCR)—The somatosensory cortex of WT and ShhcKO mice was dissected out in PBS and stored at −80C. Total RNA was extracted using the Qiagen RNeasy Mini Kit in both tissue and cell cultures. First strand synthesis was performed using Invitrogen a SuperScript III First-Strand Synthesis Kit with Oligo$(dT)_{20}$ primers (Invitrogen). Quantitative PCR was performed using Sybr Green Supermix (BIORAD) on a C1000 Touch thermocycler (BIO-RAD). Relative levels of mRNA were calculated using the delta CT method with *Gapdh* as the internal control. For RNA-seq samples, a subset of genes was confirmed by real-time PCR analysis using purified cDNA of sorted cells, Primers designed for each tested gene can be found in the key resources table.

***In utero* electroporation—**Timed pregnant mice were anesthetized using an isoflurane vaporizer and placed on a warming pad. An abdominal incision of about 1 inch in length was made and the uterine horns were carefully exposed on top of a sterile gauze pad. Embryos were kept moist with pre-warmed PBS at 37°C during the entire procedure. Approximately1-2 μL of endotoxin-free DNA (1-3 mg/ml) diluted in PBS/0.025% Fast

Author Manuscript Author Manuscript Author Manuscript Author Manuscript

Green (SIGMA) was injected into the lateral ventricles of the forebrain using heat-pulled glass micropipettes (Drummond). Once all embryos were injected, 5 pulses of 30-40 V (50 ms duration and 950 ms intervals) were applied with 7 mm platinum electrodes (BTX) connected to an ECM 830 square wave electroporator (BTX). The abdominal cavity was then sutured and stapled before administering buprenorphine (0.05-0.1 mg/kg) and ketoprofen (5-10 mg/kg). Mice were allowed to recover in a 37°C chamber after surgery. All mice were collected at P14.

Postnatal astrocytes label by electroporation (PALE)—Early postnatal (P0-P1) WT ($Shh^{flox/flox}$) and ShhcKO (Emx1-Cre; $Shh^{flox/flox}$) mice were sedated by hypothermia by being placed on ice for 4-5 min. Approximately 1 μL of endotoxin-free plasmid DNA (1 mg/ml) with Fast Green Dye was injected into the lateral ventricles of one hemisphere as described above (*In utero* Electroporation method). We used a plasmid (CAG-mTdT-2A-H2BGFP) to label nuclei with GFP and astrocyte processes with tdTomato. Following the plasmid injection, 5 discrete 50 msec pulses of 100 V were delivered at 950 msec intervals to the head of each injected pup, with the positive pole of the electrode placed on the side of the injection. Pups were covered on a 37°C pad until fully responsive, then placed back into their home cage. shRNA knockdown experiments: plasmids coding for Lrig1 shRNA, Sparc shRNA and Il33 shRNA and scrambled control were electroporated at 3 mg/ml, all shRNA and scrambled controls were combined with 2 mg/ml of pCAG-tdTomato (Addgene) to co-label the cells with GFP and tdTomato. The GFP signal was driven by CMV promoter which was silenced in a few weeks, but shRNA expression was driven by U6 promoter which allowed stable and continuous shRNA expression (Makinen et al., 2006). Samples were collected at P21.

In-vivo astrocyte complexity analysis (Sholl analysis)—High magnification 63X objective Z-stack images were obtained using a Leica SP8 confocal microscope. 5 μm-thick Z-stacks of 18 serial sections were imaged with tdTomato and GFP (WT and ShhcKO) or tdTomato (WT and Ptch1cKO) channels. Each Z-stack was converted into maximum projection images using Fiji. Sholl analysis was performed using the Sholl analysis plugin in Fiji. Starting sholl radii at 5 μm from the line start, sholl radii at 1μm increments.

Analysis of synaptic staining—For electroporated mice, P21 controls and ShhcKO sections were stained with an antibody against pre- and postsynaptic makers: VGluT1 and PSD95, VGluT2 and PSD95. High magnification (100 X 1.44 NA objective plus 1.5X optical zoom) Z-stack images were obtained with a Leica SP8 confocal microscope. Each image including individual astrocyte with 5 um-thick Z stacks. The number of co-localized synaptic puncta on top of tdTomato+ astrocyte territory was analyzed using MATLAB (see key resources table). For tamoxifen induced mice (WT and Ptch1cKO), high magnification of 2D images were obtained by a Leica Sp8 confocal microscope, the coding applies to either 2D or 3D images.

Electrophysiology—Acute Brain Slice Preparation: Brain slices were obtained from P21-P28 days old mice, WT and Ptch1cKO (both male and female) using standard techniques. Mice were anesthetized by isoflurane inhalation and perfused transcardially with ice-cold

Author Manuscript Author Manuscript Author Manuscript Author Manuscript

artificial cerebrospinal fluid (ACSF) containing (in mM) 125 NaCl, 2.5 KCl, 25 $NaHCO_3$, 2 $CaCl_2$, 1 $MgCl_2$, 1.25 NaH_2PO_4 and 25 glucose (295 mOsm/kg). Brains were blocked and transferred into a slicing chamber containing ice-cold ACSF. Coronal slices of cerebral cortex were cut at 300 μm thickness with a Leica VT1000s vibratome in ice-cold ACSF, transferred for 10 min to a holding chamber containing choline-based solution (consisting of (in mM): 110 choline chloride, 25 $NaHCO_3$, 2.5 KCl, 7 $MgCl_2$, 0.5 $CaCl_2$, 1.25 NaH_2PO_4, 25 glucose, 11.6 ascorbic acid, and 3.1 pyruvic acid) at 34C then transferred to a secondary holding chamber containing ACSF at 34°C for 10 min and subsequently maintained at room temperature (20–22°C) until use. Electrophysiology recordings: Individual brain slices were transferred into a recording chamber, mounted on an upright microscope (Olympus BX51WI) and continuously superfused (2–3 ml min^{-1}) with ACSF warmed to 32–34°C by passing it through a feedback-controlled in-line heater (SH-27B; Warner Instruments). Cells were visualized through a 60X water-immersion objective with either infrared differential interference contrast optics or epifluorescence to identify tdTomato+ cells. For whole cell voltage clamp recording, patch pipettes (2–4 MΩ) pulled from borosilicate glass (G150F-3, Warner Instruments) were filled with internal solution containing (in mM) 135 $CsMeSO_3$, 10 HEPES, 1 EGTA, 3.3 QX-314 (Cl− salt), 4 Mg-ATP, 0.3 Na-GTP, 8 Na_2-phosphocreatine (pH 7.3 adjusted with CsOH; 295 mOsm·kg–1). mEPSCs were recorded for 5min in the presence of 1 μM tetrodotoxin (Tocris) and 10 μM gabazine (Tocris) at a holding potential of −70 mV. To record evoked EPSC of pyramidal neurons in Layer V of S1 region, the membrane voltages were clamped at −70 mV, and 10 μM gabazine were added to the bath, extracellular stimulation was performed with a stimulus isolation unit (MicroProbes, ISO-Flex), bipolar electrodes (100 μm apart, PlasticOne) were placed on layer II/III of S1, 200 to 400 μm perpendicularly away from recording cells, evoke EPSC input-out curves were generated at 0.1 ms, from 10 μA at 10 μA steps to 100 μA. Data acquisition and analysis: membrane currents and potentials were amplified and low-pass filtered at 3 kHz using a Multiclamp 700B amplifier (Molecular Devices), digitized at 10 kHz and acquired using National Instruments acquisition boards and a custom version of ScanImage written in MATLAB. Electrophysiology data were analyzed offline using Igor Pro. Voltage-clamp traces represent the averaged waveform of five to seven consecutive acquisitions (Figure 6). Detection threshold for mEPSCs was set at 7 pA. Averaged waveforms were used to obtain current latency and peak amplitude. Peak amplitudes were calculated by averaging over a 2 ms window around the peak. Grubb's test was used to detect outliers in this data. Data were compared statistically by Welch's t test.

Cortical progenitor culture—Cortical progenitor cells were collected as described previously (Yuzwa et al., 2016). Pregnant CD1 mice were sacrificed at 13 days of gestation (E13) using CO_2 euthanasia. Embryos were placed in ice-cold Hank's balanced salt solution (HBSS, Gibco) and maintained on ice during dissection. Following removal of the meninges, cortices were dissected in ice-cold HBSS, and immediately placed in cortical precursor culture medium (Neurobasal medium [Gibco], 40 ng/ml FGF2 [BD Biosciences], 2% B27 supplement [Gibco], 1% Penicillin and Streptomycin [Lonza], and 500 μM L-Glutamine [Gibco]). Dissected tissue was dissociated with a sterile Pasteur pipette. Viable cells were counted via Trypan blue exclusion using a cell counter. Cells were plated at densities between 7,000 and 440,000 cells/cm^2.

Author Manuscript Author Manuscript Author Manuscript Author Manuscript

Cortical astrocyte culture—Cortices were dissected from P1 mouse pups and incubated with 0.25% trypsin-EDTA for 20 min at 37°C. Tissue was triturated and suspended in 10% FBS DMEM (Gibco). Cells were plated at a uniform density of 10-15 x10^6 cells on pre-coated flask (with 50 μg/ml Poly-D-lysine). The medium was changed every 2 to 3 days. Other glia cells were removed by shaking at 200 rpm for 2 h at 37°C. Cells were cultured for 12-14 days before being treated with shRNA.

***In vitro* shRNA transfection—**For knockdown experiments, 1 μg of scrambled or experimental shRNA (see key resources table) was used. 1.0 μL Lipofectamine and 0.5 μL Plus Reagent was prepared in Opti-MEM (Gibco) for each well of a 24-well plate, and the mix was incubated at room temperature for 5 minutes for DNA-lipid complex formation. The DNA-lipid complex was then added to the wells of precursor cultures after 7 days *in vitro* (DIV7) and DIV12 astrocytes cultures. Half of the medium was changed 16 h post-transfection. RNA extraction and RT-PCR were conducted 3 days post-transfection. All shRNA were validated by Sigma company as below: Lrig1-shRNA: mean knockdown Level: 0.75, cell line: NIH/3T3; Sparc-shRNA: mean knockdown Level: 0.86, cell line: B16-F0; Il33-shRNA: mean knockdown Level: 0.95, cell line: Hepa 1-6.

QUANTIFICATION AND STATISTICAL ANALYSIS

Cell counting was analyzed manually with ImageJ/Fiji cell counter (National Institute of Health, USA). Analysis of cell density was done in ImageJ by dividing the thickness of the cortex into five or six layers based on DAPI density, the area size of the region of interest were measured and the cells in these regions were counted. Kir4.1 intensity analysis was measured with ImageJ/Fiji, mean fluorescence intensity were measured in the region of interest after background subtraction. Sholl analysis was performed with ImageJ/Fiji. Quantification of synapse puncta in astrocyte territories and quantification of RNA puncta per unit area were carried out automatically using a data processing pipeline (see key resources table) in MATLAB R2019b. Electron microscopy images were aligned to form a 3D image volume using AlignTK software, Image volumes were accessed and annotated using the CATMAID software, 3D image data surrounding the synapse was extracted using the pymaid API, then manually segmented using itk-SNAP software. Electrophysiology data were analyzed offline using Igor Pro. Grubbs' test was performed on electrophysiology data to determine the significant outliers (Alpha=0.05). All statistical tests were performed in either Prism 8 or SPSS. Statistical analysis of astrocyte contact fraction and glycogen granules counts can be found in Table S1 and S2. Values represent mean ± SE as indicated in figure legends. For each experiment, the identity of (n) replicates is indicated in figure legends. Significance was determined using corresponding statistics test indicated in figure legends and reported as either p value or : *$p < 0.05$, **$p < 0.01$, ***$p < 0.001$.

Supplementary Material

Refer to Web version on PubMed Central for supplementary material.

Author Manuscript Author Manuscript Author Manuscript Author Manuscript

ACKNOWLEDGMENTS

The authors would like to thank Mahmoud El-Rifai and Aurélien Begué at the Neurobiology Imaging Facility, Harvard Medical School for the RNAscope experiments; Jasper Maniates-Selvin and Logan Thomas for EM technical support, David Hildebrand for help with serial section collection using GridTape, and Michelle Lowe Ocana at the Neurobiology Imaging Facility for confocal imaging technical support; Clarence Yapp at the Therapeutic Science Department, Harvard Medical School for MATLAB code; and all members of the Harwell lab. Y.X. is partially supported by Alice and Joseph Brooks Fund Fellowship and Louis Perry Jones Postdoctoral Fellowship. This research was supported by the Harvard Medical School Dean's Initiative Award for Innovation Grants in the Basic and Social Sciences. Research in C.C.H.'s laboratory is supported by NIH grants R01MH119156 and R01NS102228.

REFERENCES

Abbott NJ, Ronnback L, and Hansson E (2006). Astrocyte-endothelial interactions at the blood-brain barrier. Nat. Rev. Neurosci. 7, 41–53. 10.1038/nrn1824. [PubMed: 16371949]

Akdemir ES, Huang AY, and Deneen B (2020). Astrocytogenesis: where, when, and how. F1000Res 9. 10.12688/f1000research.22405.1.

Allahyari RV, Clark KL, Shepard KA, and Garcia ADR (2019). Sonic hedgehog signaling is negatively regulated in reactive astrocytes after forebrain stab injury. Sci. Rep. 9, 565. 10.1038/s41598-018-37555-x. [PubMed: 30679745]

Allen BL, Song JY, Izzi L, Althaus IW, Kang JS, Charron F, Krauss RS, and McMahon AP (2011). Overlapping roles and collective requirement for the coreceptors GAS1, CDO, and BOC in SHH pathway function. Dev. Cell 20, 775–787. 10.1016/j.devcel.2011.04.018. [PubMed: 21664576]

Allen NJ, and Eroglu C (2017). Cell Biology of astrocyte-synapse interactions. Neuron 96, 697–708. 10.1016/j.neuron.2017.09.056. [PubMed: 29096081]

Alsina FC, Hita FJ, Fontanet PA, Irala D, Hedman H, Ledda F, and Paratcha G (2016). Lrig1 is a cell-intrinsic modulator of hippocampal dendrite complexity and BDNF signaling. EMBO Rep. 17, 601–616. 10.15252/embr.201541218. [PubMed: 26935556]

Alvarez JI, Dodelet-Devillers A, Kebir H, Ifergan I, Fabre PJ, Terouz S, Sabbagh M, Wosik K, Bourbonniere L, Bernard M, et al. (2011). The Hedgehog pathway promotes blood-brain barrier integrity and CNS immune quiescence. Science 334, 1727–1731. 10.1126/science.1206936. [PubMed: 22144466]

Araque A, Parpura V, Sanzgiri RP, and Haydon PG (1999). Tripartite synapses: glia, the unacknowledged partner. Trends Neurosci. 22, 208–215. 10.1016/s0166-2236(98)01349-6. [PubMed: 10322493]

Baldwin KT, and Eroglu C (2017). Molecular mechanisms of astrocyte-induced synaptogenesis. Curr. Opin. Neurobiol. 45, 113–120. 10.1016/j.conb.2017.05.006. [PubMed: 28570864]

Batiuk MY, Martirosyan A, Wahis J, deVin F, Marneffe C, Kusserow C, Koeppen J, Viana JF, Oliveira JF, Voet T, et al. (2020). Identification of region-specific astrocyte subtypes at single cell resolution. Nat. Commun. 11, 1220. 10.1038/s41467-019-14198-8. [PubMed: 32139688]

Bayraktar OA, Bartels T, Holmqvist S, Kleshchevnikov V, Martirosyan A, Polioudakis D, Ben Haim L, Young AMH, Batiuk MY, Prakash K, et al. (2020).Astrocyte layers in the mammalian cerebral cortex revealed by a single-cell in situ transcriptomic map. Nat. Neurosci. 23, 500–509. 10.1038/s41593-020-0602-1. [PubMed: 32203496]

Ben Haim L, and Rowitch DH (2017). Functional diversity of astrocytes in neural circuit regulation. Nat. Rev. Neurosci. 18, 31–41. 10.1038/nrn.2016.159. [PubMed: 27904142]

Brasko C, Hawkins V, De La Rocha IC, and Butt AM (2017). Expression of Kir4.1 and Kir5.1 inwardly rectifying potassium channels in oligodendrocytes, the myelinating cells of the CNS. Brain Struct. Funct. 222, 41–59. 10.1007/s00429-016-1199-8. [PubMed: 26879293]

Bushong EA, Martone ME, Jones YZ, and Ellisman MH (2002). Protoplasmic astrocytes in CA1 stratum radiatum occupy separate anatomical domains. J. Neurosci. 22, 183–192. [PubMed: 11756501]

Author Manuscript Author Manuscript Author Manuscript Author Manuscript

Cai Y, Guo H, Fan Z, Zhang X, Wu D, Tang W, Gu T, Wang S, Yin A, Tao L, et al. (2020). Glycogenolysis is crucial for astrocytic glycogen accumulation and brain damage after reperfusion in ischemic stroke. iScience 23, 101136. 10.1016/j.isci.2020.101136. [PubMed: 32446205]

Cali C, Agus M, Kare K, Boges DJ, Lehvaslaiho H, Hadwiger M, and Magistretti PJ (2019a). 3D cellular reconstruction of cortical glia and parenchymal morphometric analysis from Serial Block-Face Electron Microscopy of juvenile rat. Prog. Neurobiol. 183, 101696. 10.1016/j.pneurobio.2019.101696. [PubMed: 31550514]

Cali C, Tauffenberger A, and Magistretti P (2019b). The strategic location of glycogen and lactate: from body energy reserve to brain plasticity. Front. Cell Neurosci. 13, 82. 10.3389/fncel.2019.00082. [PubMed: 30894801]

Clavreul S, Abdeladim L, Hernandez-Garzon E, Niculescu D, Durand J, Ieng SH, Barry R, Bonvento G, Beaurepaire E, Livet J, and Loulier K (2019). Cortical astrocytes develop in a plastic manner at both clonal and cellular levels. Nat. Commun. 10, 4884. 10.1038/s41467-019-12791-5. [PubMed: 31653848]

Cornwell M, Vangala M, Taing L, Herbert Z, Koster J, Li B, Sun H, Li T, Zhang J, Qiu X, et al. (2018). VIPER: visualization Pipeline for RNA-seq, a Snakemake workflow for efficient and complete RNA-seq analysis. BMC Bioinformatics 19, 135. 10.1186/s12859-018-2139-9. [PubMed: 29649993]

Custo Greig LF, Woodworth MB, Galazo MJ, Padmanabhan H, and Macklis JD (2013). Molecular logic of neocortical projection neuron specification, development and diversity. Nat. Rev. Neurosci. 14, 755–769. 10.1038/nrn3586. [PubMed: 24105342]

Dessaud E, McMahon AP, and Briscoe J (2008). Pattern formation in the vertebrate neural tube: a sonic hedgehog morphogen-regulated transcriptional network. Development 135, 2489–2503. 10.1242/dev.009324. [PubMed: 18621990]

Dienel GA, and Rothman DL (2019). Glycogenolysis in cerebral cortex during sensory stimulation, acute hypoglycemia, and exercise: impact on astrocytic energetics, aerobic glycolysis, and astrocyte-neuron interactions. Adv. Neurobiol. 23, 209–267. 10.1007/978-3-030-27480-1_8. [PubMed: 31667811]

Djukic B, Casper KB, Philpot BD, Chin LS, and McCarthy KD (2007). Conditional knock-out of Kir4.1 leads to glial membrane depolarization, inhibition of potassium and glutamate uptake, and enhanced short-term synaptic potentiation. J. Neurosci. 27, 11354–11365. 10.1523/JNEUROSCI.0723-07.2007. [PubMed: 17942730]

Dobin A, Davis CA, Schlesinger F, Drenkow J, Zaleski C, Jha S, Batut P, Chaisson M, and Gingeras TR (2013). STAR: ultrafast universal RNA-seq aligner. Bioinformatics 29, 15–21. 10.1093/bioinformatics/bts635. [PubMed: 23104886]

Farhy-Tselnicker I, and Allen NJ (2018). Astrocytes, neurons, synapses: a tripartite view on cortical circuit development. Neural Dev. 13, 7. 10.1186/s13064-018-0104-y. [PubMed: 29712572]

Farmer WT, Abrahamsson T, Chierzi S, Lui C, Zaelzer C, Jones EV, Bally BP, Chen GG, Theroux JF, Peng J, et al. (2016). Neurons diversify astrocytes in the adult brain through sonic hedgehog signaling. Science 351, 849–854. 10.1126/science.aab3103. [PubMed: 26912893]

Ferent J, Cochard L, Faure H, Taddei M, Hahn H, Ruat M, and Traiffort E (2014). Genetic activation of Hedgehog signaling unbalances the rate of neural stem cell renewal by increasing symmetric divisions. Stem Cell Rep. 3, 312–323. 10.1016/j.stemcr.2014.05.016.

Gadani SP, Walsh JT, Smirnov I, Zheng J, and Kipnis J (2015). The glia-derived alarmin IL-33 orchestrates the immune response and promotes recovery following CNS injury. Neuron 85, 703–709. 10.1016/j.neuron.2015.01.013. [PubMed: 25661185]

Garcia AD, Petrova R, Eng L, and Joyner AL (2010). Sonic hedgehog regulates discrete populations of astrocytes in the adult mouse forebrain.J. Neurosci. 30, 13597–13608. 10.1523/JNEUROSCI.0830-10.2010. [PubMed: 20943901]

Garcia ADR, Han YG,Triplett JW, Farmer WT, Harwell CC, and Ihrie RA (2018). The elegance of sonic hedgehog: emerging novel functions for a classic morphogen. J. Neurosci. 38, 9338–9345. 10.1523/JNEUROSCI.1662-18.2018. [PubMed: 30381425]

Author Manuscript Author Manuscript Author Manuscript Author Manuscript

Goodrich LV, Milenkovic L, Higgins KM, and Scott MP (1997). Altered neural cell fates and medulloblastoma in mouse patched mutants. Science 277, 1109–1113. 10.1126/science.277.5329.1109. [PubMed: 9262482]

Graham BJ, Hildebrand DGC, Kuan AT, Maniates-Selvin JT, Thomas LA, Shanny BL, and Lee W-CA (2019). High-throughput transmission electron microscopy with automated serial sectioning. bioRxiv. 10.1101/657346.

Hammond TR, Dufort C, Dissing-Olesen L, Giera S, Young A, Wysoker A, Walker AJ, Gergits F, Segel M, Nemesh J, et al. (2019). Single-cell RNA sequencing of microglia throughout the mouse lifespan and in the injured brain reveals complex cell-state changes. Immunity 50, 253–271 e256. 10.1016/j.immuni.2018.11.004. [PubMed: 30471926]

Harwell CC, Parker PR, Gee SM, Okada A, McConnell SK, Kreitzer AC, and Kriegstein AR (2012). Sonic hedgehog expression in corticofugal projection neurons directs cortical microcircuit formation. Neuron 73, 1116–1126. 10.1016/j.neuron.2012.02.009. [PubMed: 22445340]

Hill SA, Blaeser AS, Coley AA, Xie Y, Shepard KA, Harwell CC, Gao WJ, and Garcia ADR (2019). Sonic hedgehog signaling in astrocytes mediates cell type-specific synaptic organization. Elife 8, e45545. 10.7554/eLife.45545. [PubMed: 31194676]

Izzi L, Levesque M, Morin S, Laniel D, Wilkes BC, Mille F, Krauss RS, McMahon AP, Allen BL, and Charron F (2011). Boc and Gas1 each form distinct Shh receptor complexes with Ptch1 and are required for Shh-mediated cell proliferation. Dev. Cell 20, 788–801. 10.1016/j.devcel.2011.04.017. [PubMed: 21664577]

Jeong D, Lozano Casasbuenas D, Gengatharan A, Edwards K, Saghatelyan A, Kaplan DR, Miller FD, and Yuzwa SA (2020). LRIG1-Mediated inhibition of EGF receptor signaling regulates neural precursor cell proliferation in the neocortex. Cell Rep. 33, 108257. 10.1016/j.celrep.2020.108257. [PubMed: 33053360]

Jones EV, Bernardinelli Y, Tse YC, Chierzi S, Wong TP, and Murai KK (2011). Astrocytes control glutamate receptor levels at developing synapses through SPARC-beta-integrin interactions. J. Neurosci. 31, 4154–4165. 10.1523/JNEUROSCI.4757-10.2011. [PubMed: 21411656]

Jones EV, Bernardinelli Y, Zarruk JG, Chierzi S, and Murai KK (2018). SPARC and GluA1-containing AMPA receptors promote neuronal Health following CNS injury. Front. Cell Neurosci. 12, 22. 10.3389/fncel.2018.00022. [PubMed: 29449802]

Kikuchi T, Gonzalez-Soriano J, Kastanauskaite A, Benavides-Piccione R, Merchan-Perez A, DeFelipe J, and Blazquez-Llorca L (2020). Volume electron microscopy study of the relationship between synapses and astrocytes in the developing rat somatosensory cortex. Cereb. Cortex 30, 3427–3428. 10.1093/cercor/bhz343. [PubMed: 32142583]

Kucukdereli H, Allen NJ, Lee AT, Feng A, Ozlu MI, Conatser LM, Chakraborty C, Workman G, Weaver M, Sage EH, et al. (2011). Control of excitatory CNS synaptogenesis by astrocyte-secreted proteins Hevin and SPARC. Proc. Natl. Acad. Sci. U S A 108, E440–E449. 10.1073/pnas.1104977108. [PubMed: 21788491]

Lanjakornsiripan D, Pior BJ, Kawaguchi D, Furutachi S, Tahara T, Katsuyama Y, Suzuki Y, Fukazawa Y, and Gotoh Y (2018). Layer-specific morphological and molecular differences in neocortical astrocytes and their dependence on neuronal layers. Nat. Commun. 9, 1623. 10.1038/s41467-018-03940-3. [PubMed: 29691400]

Lee RT, Zhao Z, and Ingham PW (2016). Hedgehog signalling. Development 143, 367–372. 10.1242/dev.120154. [PubMed: 26839340]

Love MI, Huber W, and Anders S (2014). Moderated estimation of fold change and dispersion for RNA-seq data with DESeq2. Genome Biol. 15, 550. 10.1186/s13059-014-0550-8. [PubMed: 25516281]

Makinen PI, Koponen JK, Karkkainen AM, Malm TM, Pulkkinen KH, Koistinaho J, Turunen MP, and Yla-Herttuala S (2006). Stable RNA interference: comparison of U6 and H1 promoters in endothelial cells and in mouse brain. J. Gene Med. 8, 433–441. 10.1002/jgm.860. [PubMed: 16389634]

Maniates-Selvin JT, Hildebrand DGC, Graham BJ, Kuan AT, Thomas A, Nguyen T, Buhmann J, Azevedo AW, Shanny BL, Funke J, et al. (2020). Reconstruction of motor control circuits in adult Drosophila using automated transmission electron microscopy. bioRxiv. 10.1101/2020.01.10.902478.

Author Manuscript Author Manuscript Author Manuscript Author Manuscript

Marisca R, Hoche T, Agirre E, Hoodless LJ, Barkey W, Auer F, Castelo-Branco G, and Czopka T (2020). Functionally distinct subgroups of oligodendrocyte precursor cells integrate neural activity and execute myelin formation. Nat. Neurosci. 23, 363–374. 10.1038/s41593-019-0581-2. [PubMed: 32066987]

Mazare N, Oudart M, Moulard J, Cheung G, Tortuyaux R, Mailly P, Mazaud D, Bemelmans AP, Boulay AC, Blugeon C, et al. (2020). Local translation in perisynaptic astrocytic processes is specific and changes after fear conditioning. Cell Rep. 32, 108076. 10.1016/j.celrep.2020.108076. [PubMed: 32846133]

Morte B, and Bernal J (2014). Thyroid hormone action: astrocyte-neuron communication. Front. Endocrinol. 5, 82. 10.3389/fendo.2014.00082.

Pathania M, Torres-Reveron J, Yan L, Kimura T, Lin TV, Gordon V, Teng ZQ, Zhao X, Fulga TA, Van Vactor D, and Bordey A (2012). miR-132 enhances dendritic morphogenesis, spine density, synaptic integration, and survival of newborn olfactory bulb neurons. PLoS ONE 7, e38174. 10.1371/journal.pone.0038174. [PubMed: 22693596]

Pestana F, Edwards-Faret G, Belgard TG, Martirosyan A, and Holt MG (2020). No longer underappreciated: the emerging concept of astrocyte heterogeneity in neuroscience. Brain Sci. 10, 168. 10.3390/brainsci10030168.

Peterson KA, Nishi Y, Ma W, Vedenko A, Shokri L, Zhang X, McFarlane M, Baizabal JM, Junker JP, van Oudenaarden A, et al. (2012). Neural-specific Sox2 input and differential Gli-binding affinity provide context and positional information in Shh-directed neural patterning. Genes Dev. 26, 2802–2816. 10.1101/gad.207142.112. [PubMed: 23249739]

Reimand J, Kull M, Peterson H, Hansen J, and Vilo J (2007). g:Profiler–a web-based toolset for functional profiling of gene lists from large-scale experiments. Nucleic Acids Res. 35, W193–W200. 10.1093/nar/gkm226. [PubMed: 17478515]

Rivell A, Petralia RS, Wang YX, Clawson E, Moehl K, Mattson MP, and Yao PJ (2019). Sonic hedgehog expression in the postnatal brain. Biol. Open 8. 10.1242/bio.040592.

Rohatgi R, Milenkovic L, and Scott MP (2007). Patched1 regulates hedgehog signaling at the primary cilium. Science 317, 372–376. 10.1126/science.1139740. [PubMed: 17641202]

Saalfeld S, Cardona A, Hartenstein V, and Tomancak P (2009). CATMAID: collaborative annotation toolkit for massive amounts of image data. Bioinformatics 25, 1984–1986. 10.1093/bioinformatics/btp266. [PubMed: 19376822]

Sanders TA, Llagostera E, and Barna M (2013). Specialized filopodia direct long-range transport of SHH during vertebrate tissue patterning. Nature 497, 628–632. 10.1038/nature12157. [PubMed: 23624372]

Schindelin J, Arganda-Carreras I, Frise E, Kaynig V, Longair M, Pietzsch T, Preibisch S, Rueden C, Saalfeld S, Schmid B, et al. (2012). Fiji: an open-source platform for biological-image analysis. Nat. Methods 9, 676–682. 10.1038/nmeth.2019. [PubMed: 22743772]

Schneider-Mizell CM, Gerhard S, Longair M, Kazimiers T, Li F, Zwart MF, Champion A, Midgley FM, Fetter RD, Saalfeld S, and Cardona A (2016). Quantitative neuroanatomy for connectomics in Drosophila. Elife 5, e12059. 10.7554/eLife.12059. [PubMed: 26990779]

Singh SK, Stogsdill JA, Pulimood NS, Dingsdale H, Kim YH, Pilaz LJ, Kim IH, Manhaes AC, Rodrigues WS Jr., Pamukcu A, et al. (2016).Astrocytes assemble thalamocortical synapses by bridging NRX1alpha and NL1 via Hevin. Cell 164, 183–196. 10.1016/j.cell.2015.11.034. [PubMed: 26771491]

Stogsdill JA, Ramirez J, Liu D, Kim YH, Baldwin KT, Enustun E, Ejikeme T, Ji RR, and Eroglu C (2017). Astrocytic neuroligins control astrocyte morphogenesis and synaptogenesis. Nature 551, 192–197. 10.1038/nature24638. [PubMed: 29120426]

Sung HY, Chen WY, Huang HT, Wang CY, Chang SB, and Tzeng SF (2019). Down-regulation of interleukin-33 expression in oligodendrocyte precursor cells impairs oligodendrocyte lineage progression. J. Neurochem. 150, 691–708. 10.1111/jnc.14788. [PubMed: 31165473]

Supek F, Bosnjak M, Skunca N, and Smuc T (2011). REVIGO summarizes and visualizes long lists of gene ontology terms. PLoS ONE 6, e21800. 10.1371/journal.pone.0021800. [PubMed: 21789182]

Tong X, Ao Y, Faas GC, Nwaobi SE, Xu J, Haustein MD, Anderson MA, Mody I, Olsen ML, Sofroniew MV, and Khakh BS (2014).Astrocyte Kir4.1 ion channel deficits contribute to neuronal

Author Manuscript Author Manuscript Author Manuscript Author Manuscript

dysfunction in Huntington's disease model mice. Nat. Neurosci. 17, 694–703. 10.1038/nn.3691. [PubMed: 24686787]

Trapnell C, Williams BA, Pertea G, Mortazavi A, Kwan G, van Baren MJ, Salzberg SL, Wold BJ, and Pachter L (2010). Transcript assembly and quantification by RNA-Seq reveals unannotated transcripts and isoform switching during cell differentiation. Nat. Biotechnol. 28, 511–515. 10.1038/nbt.1621. [PubMed: 20436464]

Trichas G, Begbie J, and Srinivas S (2008). Use of the viral 2A peptide for bicistronic expression in transgenic mice. BMC Biol. 6, 40. 10.1186/1741-7007-6-40. [PubMed: 18793381]

Vainchtein ID, Chin G, Cho FS, Kelley KW, Miller JG, Chien EC, Liddelow SA, Nguyen PT, Nakao-Inoue H, Dorman LC, et al. (2018). Astrocyte-derived interleukin-33 promotes microglial synapse engulfment and neural circuit development. Science 359, 1269–1273. 10.1126/science.aal3589. [PubMed: 29420261]

Yam PT, Langlois SD, Morin S, and Charron F (2009). Sonic hedgehog guides axons through a noncanonical, Src-family-kinase-dependent signaling pathway. Neuron 62, 349–362. 10.1016/j.neuron.2009.03.022. [PubMed: 19447091]

Yushkevich PA, Piven J, Hazlett HC, Smith RG, Ho S, Gee JC, and Gerig G (2006). User-guided 3D active contour segmentation of anatomical structures: significantly improved efficiency and reliability. Neuroimage 31 ,1116–1128. 10.1016/j.neuroimage.2006.01.015. [PubMed: 16545965]

Yuzwa SA, Yang G, Borrett MJ, Clarke G, Cancino GI, Zahr SK, Zandstra PW, Kaplan DR, and Miller FD (2016). Proneurogenic ligands defined by modeling developing cortex growth factor communication networks. Neuron 91, 988–1004. 10.1016/j.neuron.2016.07.037. [PubMed: 27545711]

Zhang Y, Chen K, Sloan SA, Bennett ML, Scholze AR, O'Keeffe S, Phatnani HP, Guarnieri P, Caneda C, Ruderisch N, et al. (2014). An RNA-sequencing transcriptome and splicing database of glia, neurons, and vascular cells of the cerebral cortex. J. Neurosci. 34, 11929–11947. 10.1523/JNEUROSCI.1860-14.2014. [PubMed: 25186741]

Zhao C, and Gammie SC (2015). Metabotropic glutamate receptor 3 is downregulated and its expression is shifted from neurons to astrocytes in the mouse lateral septum during the postpartum period. J. Histochem. Cytochem 63, 417–426. 10.1369/0022155415578283. [PubMed: 25739438]

Zhao C, Teng EM, Summers RG Jr., Ming GL, and Gage FH (2006). Distinct morphological stages of dentate granule neuron maturation in the adult mouse hippocampus. J. Neurosci. 26, 3–11. 10.1523/JNEUROSCI.3648-05.2006. [PubMed: 16399667]

Author Manuscript Author Manuscript Author Manuscript Author Manuscript

Highlights

- Shh and Ptch1 are expressed by neurons and astrocytes, respectively
- Neuron-derived Shh is required for astrocyte morphogenesis and synapse ensheathment
- Shh signaling in astrocytes promotes synapse formation
- Lrig1 and Sparc distinctly contribute to astrocyte morphogenesis and synapse formation

Author Manuscript Author Manuscript Author Manuscript Author Manuscript

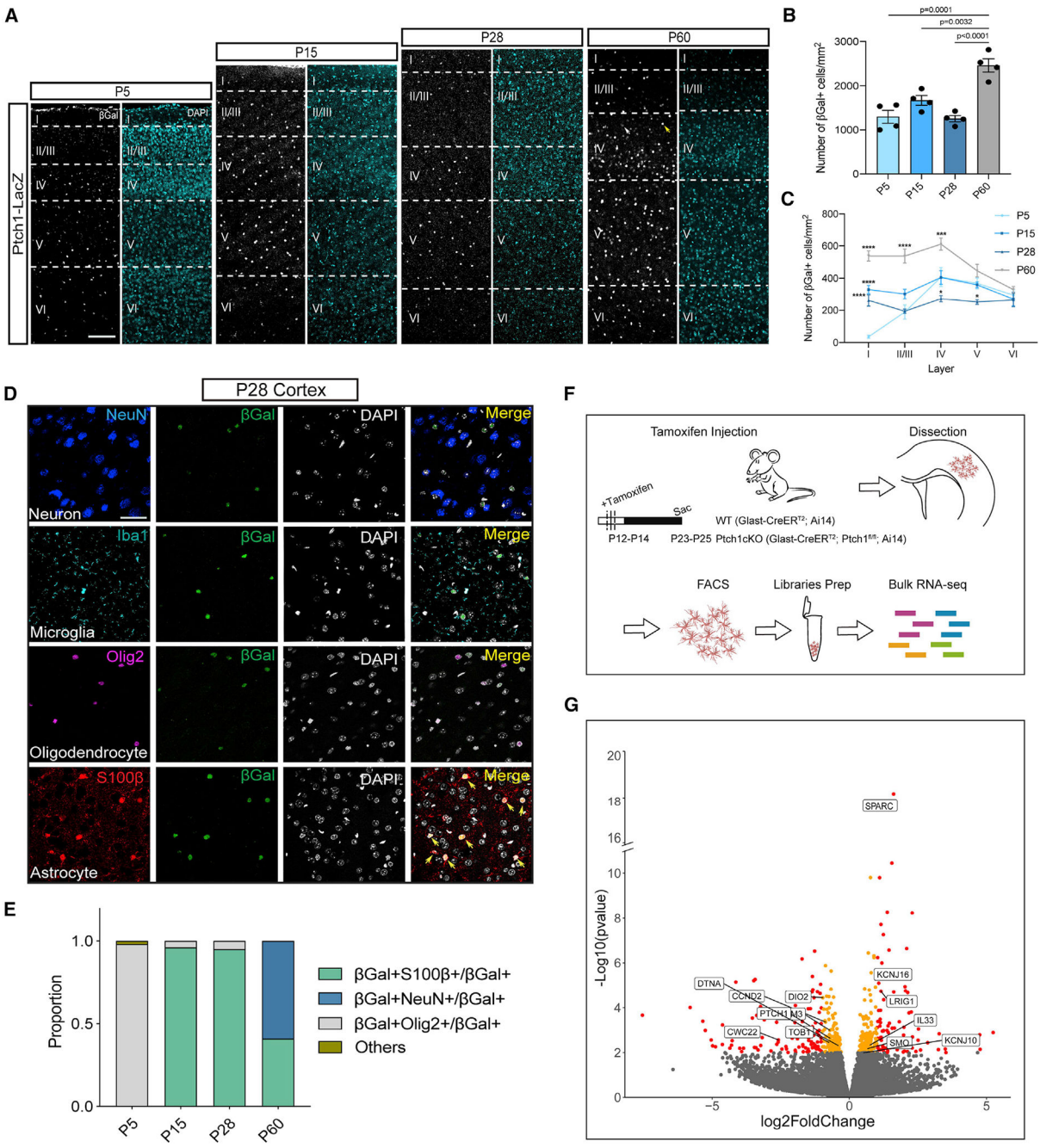

Figure 1. Ptch1 is specifically expressed in cortical astrocytes during development

(A) Immunostaining for βGal in cortical layers of P5–P60 Ptch1-LacZ mice. White and yellow arrows indicate cells with low and high βGal intensity, respectively. Scale bar, 250 μm.

(B) Density of βGal^{+} in developing cortex. n = 4 mice for each age.

(C) Density of βGal^{+} cells in each cortical layer. The density of βGal^{+} cells in P15, P28, and P60 cortex, respectively are compared with P5 cortex. n = 4 mice for each age.

Author Manuscript Author Manuscript Author Manuscript Author Manuscript

(D) Immunostaining for cell-type markers combined with βGal and DAPI in P28 Ptch1-LacZ cortex. Yellow arrows indicate representative $S100\beta^{+}\beta Gal^{+}$ cells. Scale bar, 50 μm.
(E) Proportion of Ptch1-LacZ-expressing cells with corresponding markers in P5-P60 cortex. n = 3 mice for each age.
(F) Experimental design for transcriptional profiling of WT and Ptch1cKO cortical astrocytes.
(G) Volcano plot showing fold changes of gene expression in Ptch1cKO astrocytes. Red dots, $p < 0.01$, $|\log_2 FoldChange| > 1$; orange dots, $p < 0.01$; remaining dots are gray.
Data in (B) and (C) represent mean ± SEM; statistical analyses were one-way ANOVA with Tukey's multiple comparisons test (B) and two-way ANOVA with Dunnett's multiple comparisons test (C). Only p values of <0.05 are shown. *p < 0.05, **p < 0.01, ***p < 0.001; n.s., not significant. See also Figures S1 and S2.

Author Manuscript Author Manuscript Author Manuscript Author Manuscript

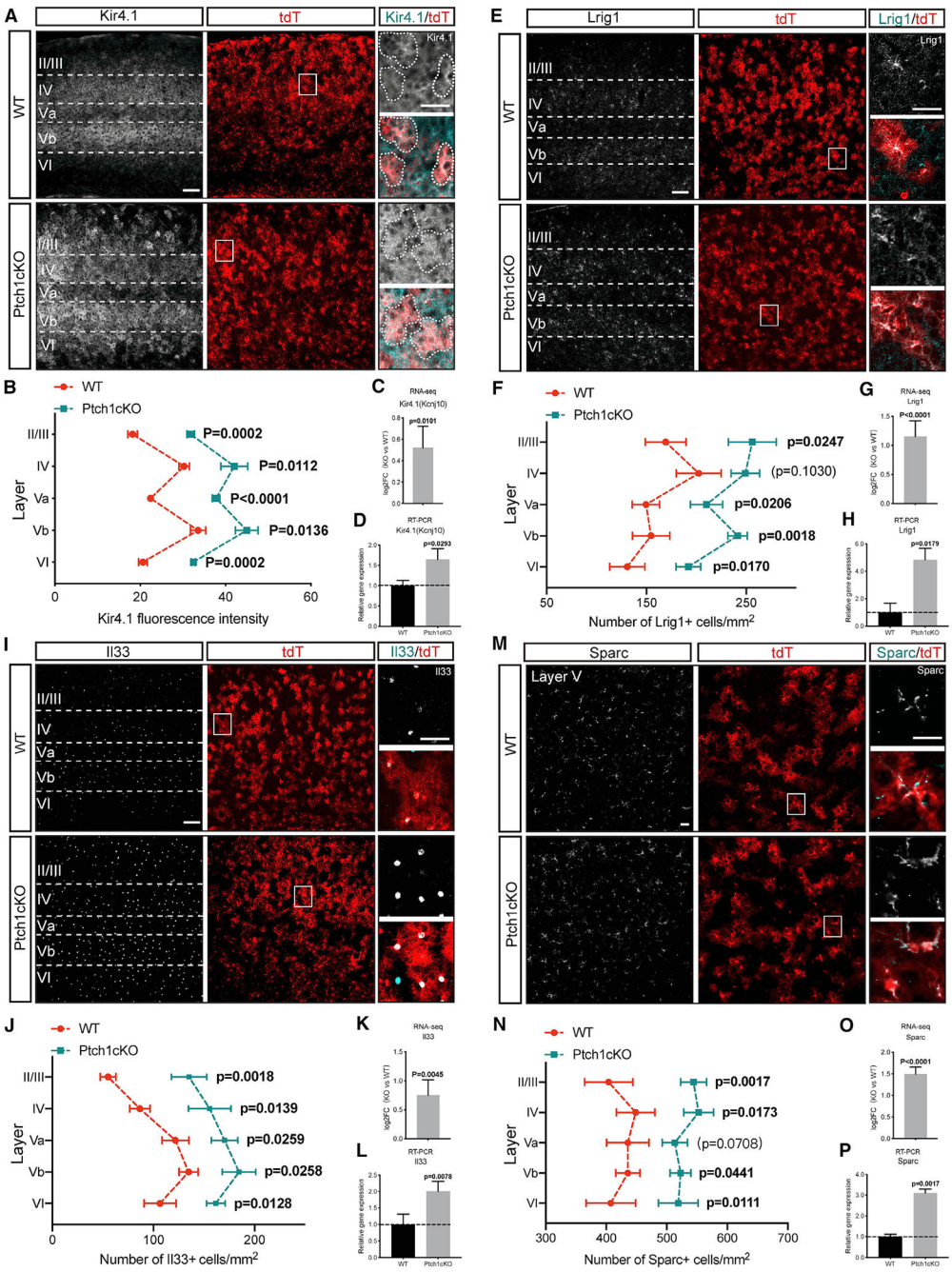

Figure 2. Expression of Shh target genes is upregulated in Ptch1cKO astrocytes

(A and B) Kir4.1 fluorescence intensity in WT and Ptch1cKO cortex. n = 4 mice for each condition. Scale bar, 100 μm.

(C, G, K, and O) RNA-seq fold change of Shh target genes in Ptch1cKO astrocytes compared with WT. n = 4 mice for each condition.

(D, H, L, and P) Real-time PCR measurement of Shh target genes in FACS-sorted tdTomato^{+} astrocytes of WT and Ptch1cKO. n = 4 mice for each condition.

Author Manuscript Author Manuscript Author Manuscript Author Manuscript

(E and F) Density of Lrig1^{+} cells in WT and Ptch1cKO cortex. WT: n = 5 mice, KO: n = 6 mice. Scale bar, 100 μm.

(I and J) Density of Il33^{+} cells in WT and Ptch1cKO cortex. n = 6 mice for each condition. Scale bar, 100 μm.

(M and N) Density of Sparc^{+} cells in WT and Ptch1cKO layer V cortex. n = 5 mice for each condition. Scale bar, 30 μm.

Data represent mean ± SEM; statistical analyses were t test (D, H, L, P) or multiple t test (B, F, J, N). See also Figures S3 and S1’4.

Author Manuscript Author Manuscript Author Manuscript Author Manuscript

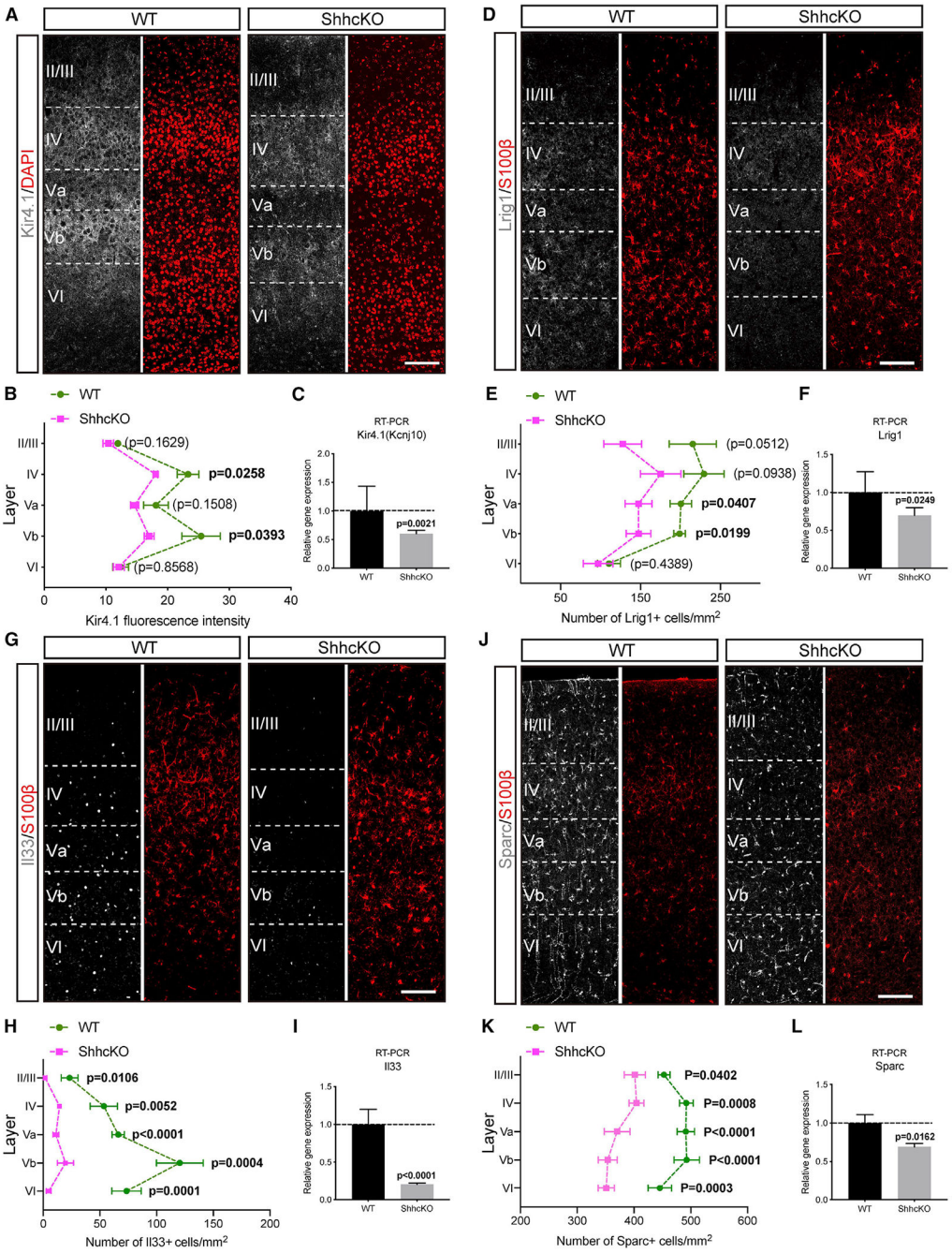

Figure 3. Expression of target genes is downregulated in ShhcKO

(A and B) Fluorescence intensity of Kir4.1 in P21 WT and ShhcKO cortex. n = 4 mice for each condition.

(C, F, I, and L) Real-time PCR shows relative gene expression of Kir4.1/Kcnj10 (C), Lrig1 (F), Il33 (I), and Sparc (L) from WT and ShhcKO cortex. n = 4 for each condition.

(D, E, G, H, J, and K) Density of Lrig1^{+} cells (D, E), Il33^{+} cells (G, H), and Sparc^{+} cells (J, K) in P21 WT and ShhcKO cortex. Lrig1: WT, n = 6 mice; KO, n = 5 mice. Il33: WT, n = 6 mice; KO, n = 7 mice. Sparc: WT, n = 3 mice; KO, n = 4 mice.

Author Manuscript Author Manuscript Author Manuscript Author Manuscript

Data represent mean ± SEM; statistical analyses were t test (C, F, I, L) or multiple t test (B, E, H, K). Scale bars, 100 μm. See also Figure S5.

Author Manuscript Author Manuscript Author Manuscript Author Manuscript

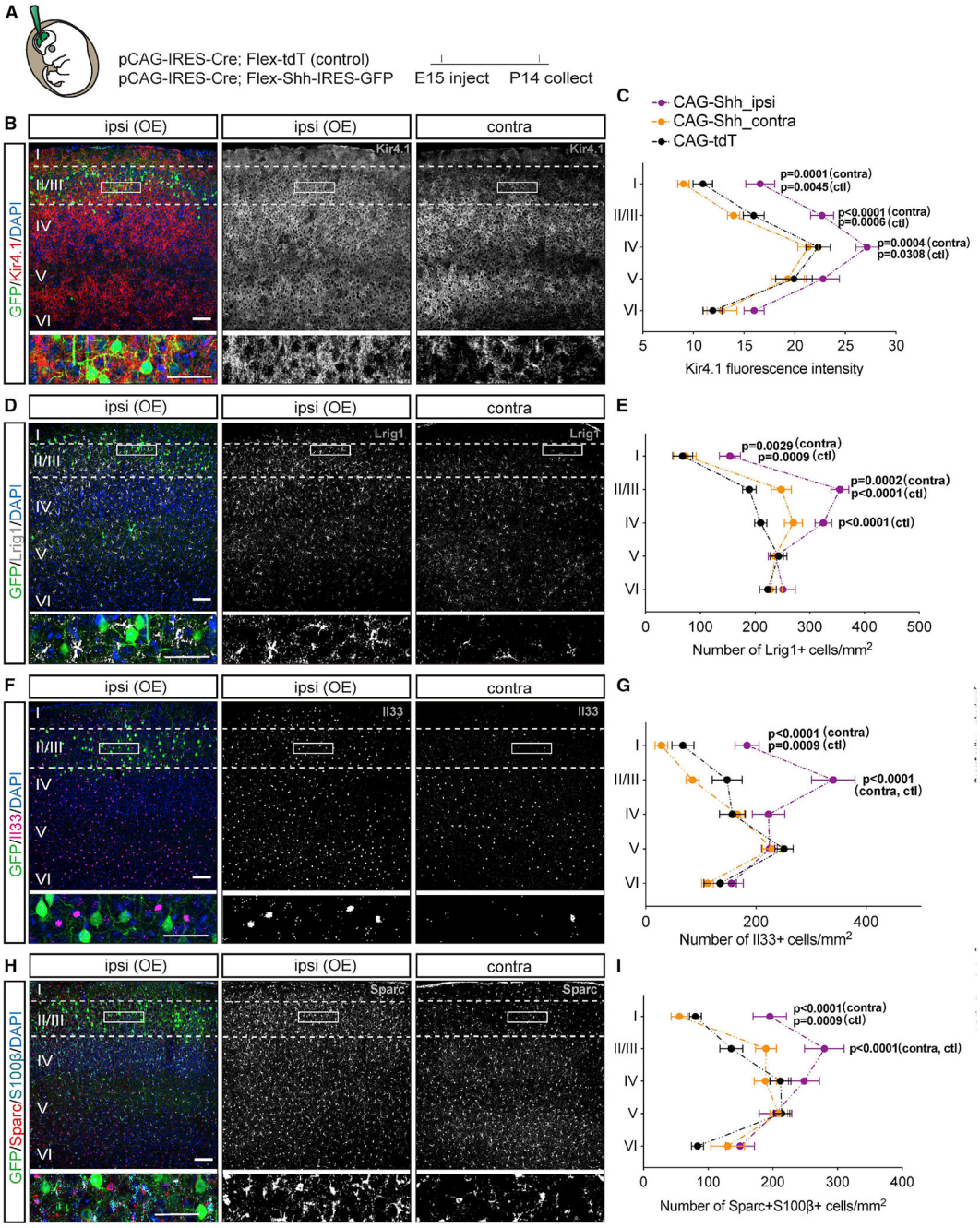

Figure 4. Ectopic expression of Shh in upper-layer neurons increases the expression of target genes in astrocytes

(A) Schematic of *in utero* electroporation in E15 embryos with control and Shh full-length plasmids.

(B–I) Immunostaining analysis of Kir4.1 fluorescence intensity (B, C), number of Lrig1$^+$ cells (D, E), number of Il33$^+$ cells (F, G), and number of Sparc$^+$S100β$^+$ cells (H, I) in Shh plasmid electroporated hemispheres compared with non-electroporated contralateral hemispheres and electroporated controls. n = 5–7 mice for each group. Scale bar, 100

μm. Data represent mean ± SEM; statistical analyses were two-way ANOVA with Tukey's multiple comparisons test (C, E, G, I).

Author Manuscript Author Manuscript Author Manuscript Author Manuscript

Author Manuscript Author Manuscript Author Manuscript Author Manuscript

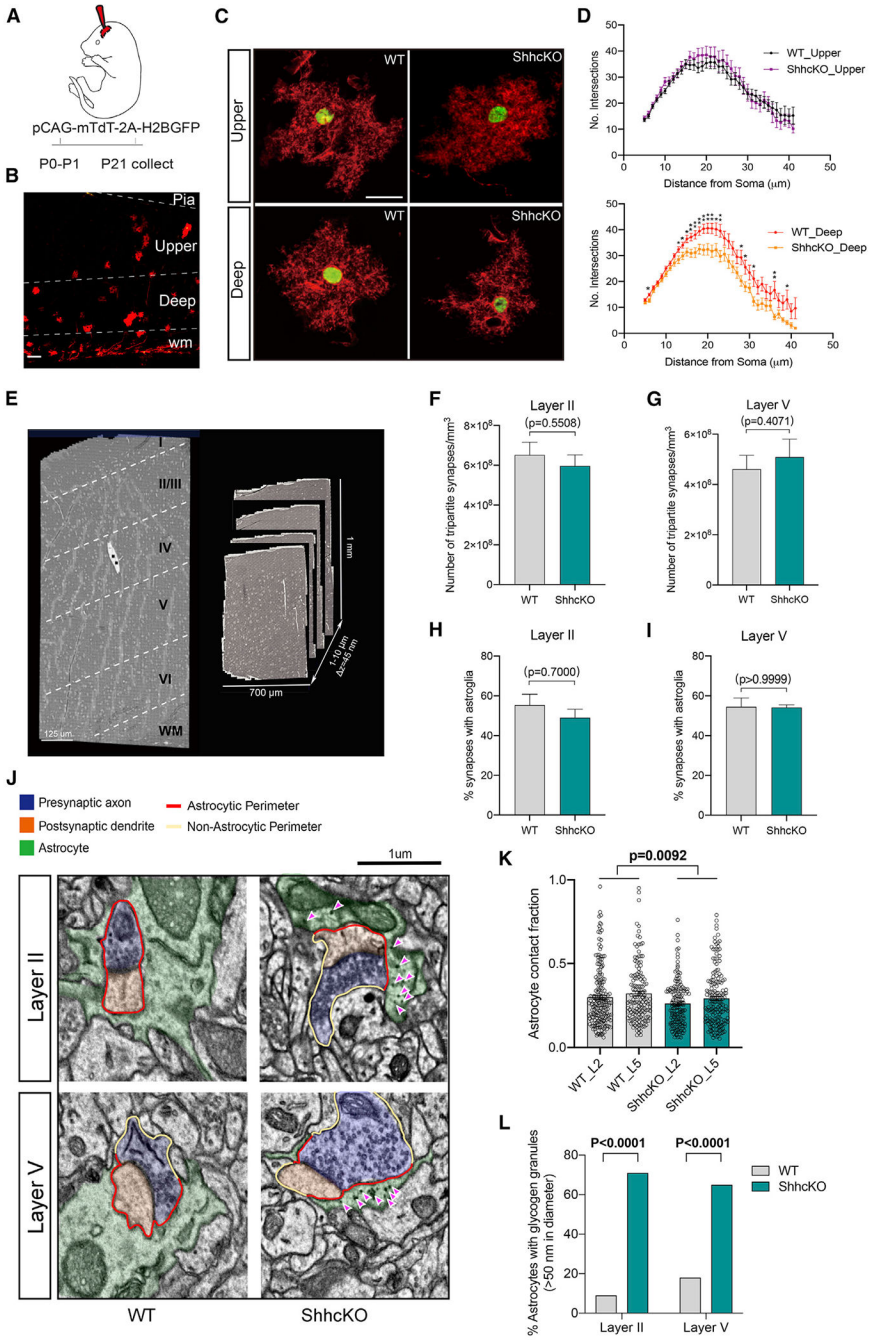

Figure 5. Deletion of Shh reduces astrocyte morphological complexity and coverage of neuronal synapses

(A) Schematic of PALE with pCAG-mTdT-2A-H2BGFP in early postnatal mice.

(B) Astrocytes were labeled with tdTomato (processes) and GFP (nuclei) in cortex after PALE. Scale bar, 100 μm.

(C) Electroporated astrocytes from upper and deep layers of WT and ShhcKO. Scale bar, 20 μm.

(D) Quantification of astrocyte complexity for deep-layer and upper-layer astrocytes.

Author Manuscript Author Manuscript Author Manuscript Author Manuscript

(E) Representative electron microscope image of serial sections from P26 WT mice. Scale bar, 125 μm.

(F and G) Density of tripartite synapses in layer II (F) or layer V (G) of WT and ShhcKO cortex.

(H and I) Proportion of tripartite synapses in layer II (H) or layer V (I) of WT and ShhcKO cortex.

(J) Representative electron microscopy images acquired from layer II and layer V cortex of WT and ShhcKO. Magenta arrows indicate dark glycogen granules in astrocytic processes. Scale bar, 1 μm.

(K) Quantification of astrocyte ensheathment of synapses in layer II and layer V cortex of WT and ShhcKO. Layer II: WT (n = 194 synapses), KO (n = 162 synapses); Layer V: WT (n = 142 synapses), KO (n = 166 synapses).

(L) Proportion of astrocytes with intensely labeled glycogen granules (>50 nm in diameter). Data represent mean ± SEM; statistical analyses were multiple t test (D), Welch's test (F, G), Mann-Whitney test (H, I), two-way ANOVA test (K), or chi-squared test (L). See also Figure S6; Tables S1 and S2.

Author Manuscript Author Manuscript Author Manuscript Author Manuscript

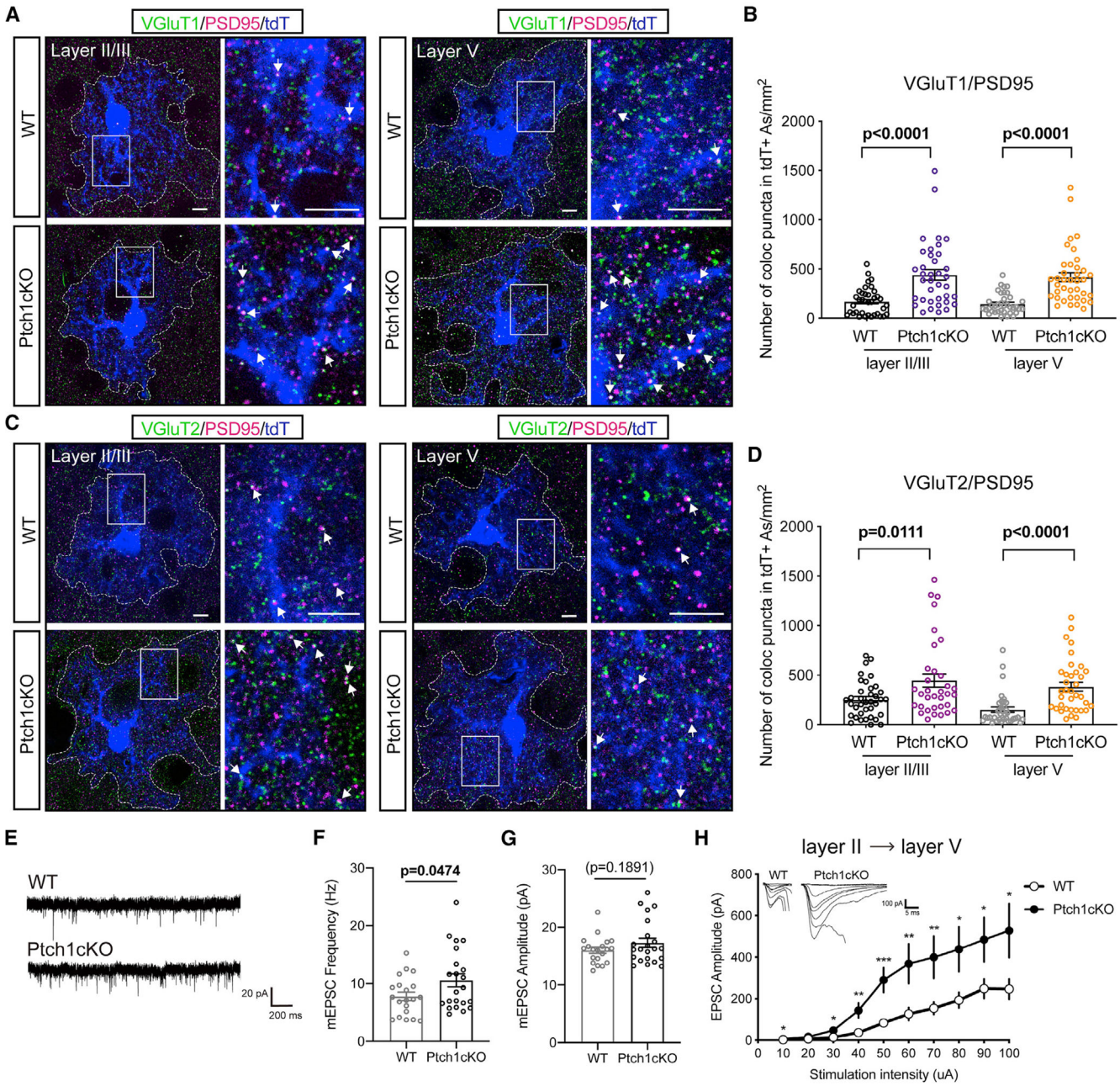

Figure 6. Loss of Ptch1 in astrocytes promotes cortical synaptogenesis

(A and C) Immunostaining for VGluT1/PSD95 (A) and VGluT2/PSD95 excitatory synapses (C) in layers II/III and layer V of WT and Ptch1cKO cortical astrocytes. Scale bar, 5 μm.

(B and D) Quantification of co-localized puncta density in tdTomato^{+} astrocyte domains per mm^{2}. N = 4 mice for each condition.

(E–G) Recordings of mEPSC from layer V neurons in WT and Ptch1cKO. N = 3 mice for each condition (WT: n = 20 cells; KO: n = 22 cells).

(H) Recordings of evoked EPSC from layer V neurons of WT and Ptch1cKO cortex. N = 4 mice for each condition (WT: n = 20 cells; KO: 15 cells).

Author Manuscript Author Manuscript Author Manuscript Author Manuscript

Data represent mean ± SEM; statistical analyses were Welch's t test (B, D, F, G) or multiple t test (H). *p < 0.05, **p < 0.01, ***p < 0.001; n.s., not significant. See also Figure S7.

Author Manuscript Author Manuscript Author Manuscript Author Manuscript

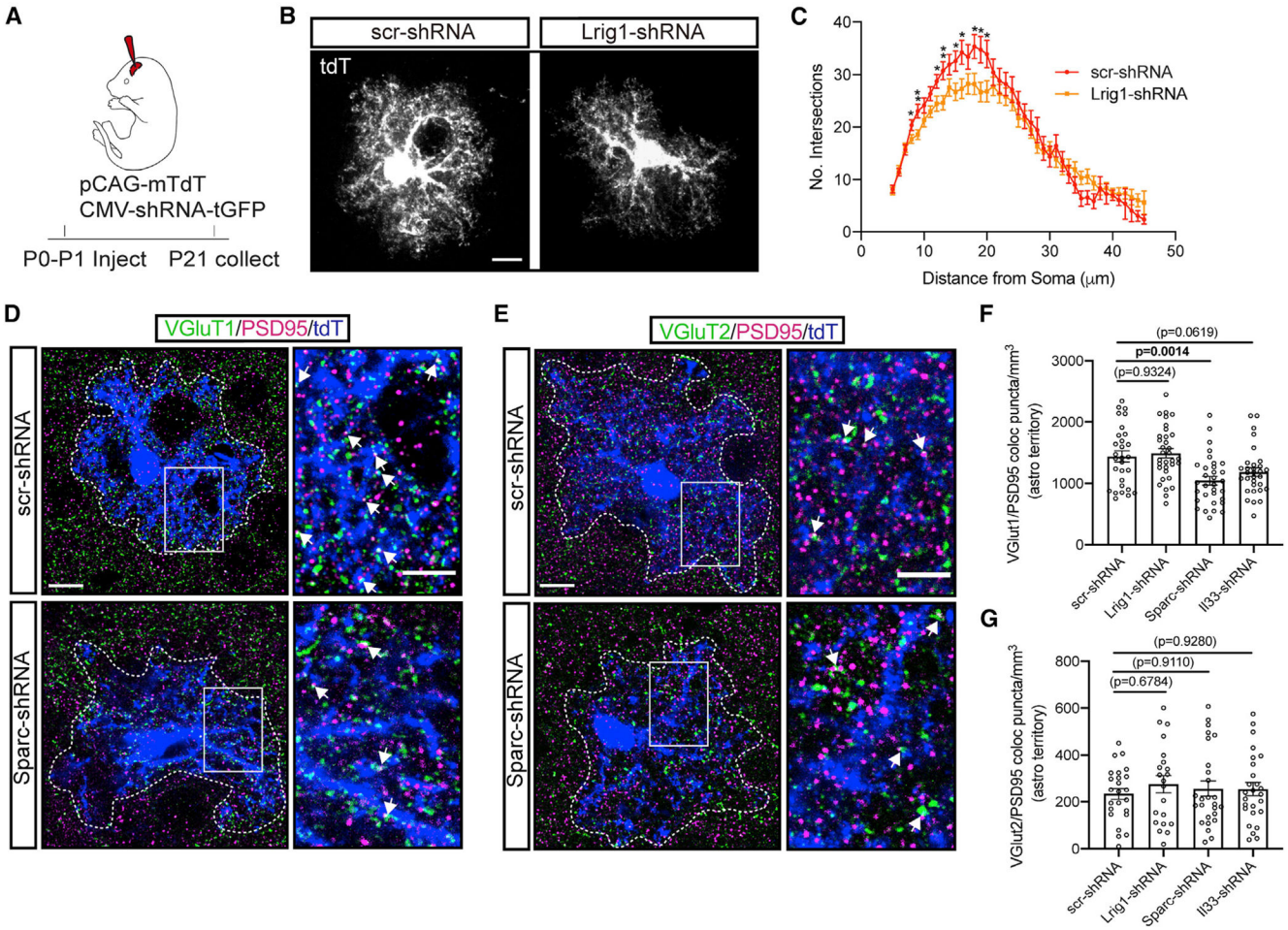

Figure 7. Knockdown of Shh-dependent genes Lrig1 and Sparc in astrocytes reduces astrocyte complexity and synapse formation, respectively

(A) Schematic of PALE with CMV-shRNA-tGFP and pCAG-mTdT in postnatal mice.

(B) P21 PALE astrocytes from deep layers of scramble-shRNA and Lrig1-shRNA groups. Scale bar, 10 μm.

(C) Sholl analysis of scramble-shRNA and Lrig1-shRNA astrocytes. scr-shRNA: n = 4 mice; Lrig1-shRNA: n = 6 mice; each group includes 26–35 cells (z stack).

(D and E) Immunostaining for VGluT1/PSD95 (D) and VGluT2/PSD95 (E) excitatory synapses in P21 scr-shRNA and Sparc-shRNA groups. Scale bar, 10 μm.

(F and G) Quantification of co-localized puncta density in tdTomato^{+} astrocyte domains. scr-shRNA: n = 4 mice; Lrig1-shRNA: n = 6 mice; Sparc-shRNA: n = 6 mice; Il33-shRNA: n = 7 mice; each V1 group includes 29–33 cells (z stack) and each V2 group includes 23–26 cells.

Data represent mean ± SEM; statistical analyses were multiple t test (C) or one-way ANOVA (F, G). See also Figure S8.

Author Manuscript Author Manuscript Author Manuscript Author Manuscript

KEY RESOURCES TABLE

REAGENT or RESOURCE	SOURCE	IDENTIFIER
Antibodies		
Mouse monoclonal anti-S100β	Sigma Aldrich	S2532; RRID:AB_477499
Mouse monoclonal anti-NeuN	Millipore	MAB377; RRID:AB_2298772
Mouse monoclonal anti-VGluT2	Millipore	MAB5504; RRID:AB_10677395
Goat monoclonal anti-Lrig1	Novus Bio	AF3688; RRID:AB_2138836
Goat monoclonal anti-Il33	Novus Bio	AF3626; RRID:AB_884269
Goat monoclonal anti-Sparc	R&D Systems	AF942; RRID:AB_2286625
Rabbit monoclonal anti-Kir4.1	Millipore	AB5818; RRID:AB_92052
Rabbit monoclonal anti-Olig2	Millipore	AB9610; RRID:AB_570666
Rabbit monoclonal anti-Iba1	Wako	019-19741; RRID:AB_839504
Chicken monoclonal anti-βGal	Aves	BGL-1040; RRID:AB_2313507
Rabbit monoclonal anti-PSD95	Thermo Fisher	51-6900; RRID:AB_2533914
Guinea pig monoclonal anti-VGluT1	Millipore	AB5905; RRID:AB_2301751
Chicken polyclonal anti-GFP	Aves	Cat # GFP-1020; RRID:AB_10000240
Chicken polyclonal anti-RFP	Rockland	Cat # 600-901-379; RRID:AB_10704808
Goat polyclonal anti-chicken Alexa 488	Thermo Fisher	Cat # A11039; RRID:AB_142924
Goat polyclonal anti-chicken Alexa 546	Thermo Fisher	Cat # A11040; RRID:AB_1500590
Goat polyclonal anti-Guinea pig Alexa 488	Thermo Fisher	Cat # A11073; RRID:AB_2534117
Goat polyclonal anti-mouse Alexa 488	Thermo Fisher	Cat # A11001; RRID:AB_2534069
Goat polyclonal anti-mouse Alexa 647	Thermo Fisher	Cat # A21236; RRID:AB_2535805
Goat polyclonal anti-rabbit Alexa 488	Thermo Fisher	Cat # A11034; RRID:AB_2576217
Goat polyclonal anti-rabbit Alexa 647	Thermo Fisher	Cat # A21245; RRID:AB_141775
Donkey polyclonal anti-goat Alexa 647	Thermo Fisher	Cat # A21447; RRID:AB_141844
Donkey polyclonal anti-mouse Alexa 488	Thermo Fisher	Cat # A21202; RRID:AB_141607
Recombinant DNA		

Author Manuscript Author Manuscript Author Manuscript Author Manuscript

REAGENT or RESOURCE	SOURCE	IDENTIFIER
pCAG-mTdT-2A-H2BGFP	Trichas et al. (2008)	Addgene #26771
pCAG-IRES-Cre	Zhao et al. (2006)	Addgene #48201
Flex-Shh-IRES-GFP	This manuscript	N/A
Flex-tdTomato	This manuscript	N/A
pCAG-tdTomato	Pathania et al. (2012)	Addgene #83029
Critical commercial assays		
Ovation Ultralow System V2 1-16	NuGEN	Cat # 0344
Ovation RNA-seq System V2	NuGEN	Cat # 7102
RNAscope Fluorescent Multiplex Assay	ACD	Document # 320513-USM; Document #
Part 1 and Part 2		320293
RNeasy Mini Kit	Qiagen	Cat# 74106
Deposited data		
RNA-seq data	This manuscript	GEO: GSE192896
MATLAB code for colocalized synaptic puncta in astrocyte territories	This manuscript	https://doi.org/10.5281/zenodo.5879992
MATLAB code for RNAscope analysis	This manuscript	https://doi.org/10.5281/zenodo.5903373
Experimental models: Organisms/strains		
Mouse: CD1	Charles river laboratories	Strain code: 022
Mouse: B6.129S6-*Shh*$^{tm2(cre/ERT2)Cjt}$/J(Shh-CreER^{T2})	The Jackson Laboratory	Stock No: 005623
Mouse: Emx1$^{IRES\ cre}$	The Jackson Laboratory	Stock No: 005628
Mouse: B6;129-*Shh*^{tm2Amc}/J(Shh$^{flox/flox}$)	The Jackson Laboratory	Stock No: 004293
Mouse: B6.Cg-*Gt*(*ROSA*) *26Sor*$^{tm14(CAG-tdTomato)Hze}$/J (Ai14)	The Jackson Laboratory	Stock No: 007914
Mouse: Tg(Slc1a3-cre/ERT)1Nat/J (Glast-CreER^{T2})	The Jackson Laboratory	Stock No: 012586
Mouse: B6N.129-*Ptch1*^{tm1Hahn}/J (Ptch1$^{flox/flox}$)	The Jackson Laboratory	Stock No: 012457
Mouse: *Ptch1*^{tm1Mps}/J(Ptch1-LacZ)	The Jackson Laboratory	Stock No: 003081
Oligonucleotides		
CMV-Non-target-shRNA-tGFP: CCGGGCGCGATAGCGCTAATAATTTCTCGAGAAATTATTAGCGCTATCGCGCTTTTT	Sigma Mission	N/A
CMV-Lrig1-shRNA-tGFP: CCGGGCGTCACTAACACAGATGAAACTCGAGTTTCATCTGTGTTAGTGACGCTTTTTG	Sigma Mission	SHCLND-NM_008377
CMV-Il33-shRNA-tGFP: CCGGGCATCCAAGGAACTTCACTTTCTCGAGAAAGTGAAGTTCCTTGGATGCTTTTTTG	Sigma Mission	SHCLND-NM_133775

Author Manuscript Author Manuscript Author Manuscript Author Manuscript

REAGENT or RESOURCE	SOURCE	IDENTIFIER
CMV-Sparc-shRNA-tGFP: CCGGGAAGGTATGCAGCAATGACAACTCGAGTTGTCATTGCTGCATACCTTCTTTTTG	Sigma Mission	SHCLND-NM_009242
Real-Time PCR, *in situ* hybridization (RNAscope)	This manuscript	Table S3
Software and algorithms		
Fiji 2.0.0-rc-69/1.52p	Schindelin et al. (2012)	https://imagej.net/Fiji
Prism 8	GraphPad	https://www.graphpad.com/scientific-software/prism/
MATLAB R2019b	Mathworks	https://www.mathworks.com/products.html
Igor Pro	Wavemetrics	https://www.wavemetrics.com/
itk-SNAP	Yushkevich et al. (2006)	www.itksnap.org
STAR	Dobin et al. (2013)	https://code.google.com/archive/p/rna-star/
DESeq2	Love et al. (2014)	http://www.bioconductor.org/packages/release/bioc/html/DESeq2.html
REVIGO	Supek et al., (2011)	http://revigo.irb.hr/
gProfiler	Reimand et al. (2007)	http://biit.cs.ut.ee/gprofiler/gost
CATMAID	Saalfeld et al. (2009) and Schneider-Mizell et al. (2016)	https://catmaid.readthedocs.io/en/stable/
AlignTK	National Center for Multiscale Modeling of Biological Systems	https://mmbios.pitt.edu/aligntk-home